JCI The Journal of Clinical Investigation

Podocyte histone deacetylase activity regulates murine and human glomerular diseases

Kazunori Inoue, … , Francis P. Wilson, Shuta Ishibe

J Clin Invest. 2019;129(3):1295-1313. https://doi.org/10.1172/JCI124030.

Research Article **Cell biology** **Nephrology**

We identified 2 genes, histone deacetylase 1 (*HDAC1*) and *HDAC2*, contributing to the pathogenesis of proteinuric kidney diseases, the leading cause of end-stage kidney disease. mRNA expression profiling from proteinuric mouse glomeruli was linked to Connectivity Map databases, identifying *HDAC1* and *HDAC2* with the differentially expressed gene set reversible by HDAC inhibitors. In numerous progressive glomerular disease models, treatment with valproic acid (a class I HDAC inhibitor) or SAHA (a pan-HDAC inhibitor) mitigated the degree of proteinuria and glomerulosclerosis, leading to a striking increase in survival. Podocyte HDAC1 and HDAC2 activities were increased in mice podocytopathy models, and podocyte-associated *Hdac1* and *Hdac2* genetic ablation improved proteinuria and glomerulosclerosis. Podocyte early growth response 1 (EGR1) was increased in proteinuric patients and mice in an HDAC1- and HDAC2-dependent manner. Loss of EGR1 in mice reduced proteinuria and glomerulosclerosis. Longitudinal analysis of the multicenter Veterans Aging Cohort Study demonstrated a 30% reduction in mean annual loss of estimated glomerular filtration rate, and this effect was more pronounced in proteinuric patients receiving valproic acid. These results strongly suggest that inhibition of HDAC1 and HDAC2 activities may suppress the progression of human proteinuric kidney diseases through the regulation of EGR1.

Podocyte histone deacetylase activity regulates murine and human glomerular diseases

Kazunori Inoue,[1] Geliang Gan,[2] Maria Ciarleglio,[2] Yan Zhang,[3,4,5] Xuefei Tian,[1] Christopher E. Pedigo,[1] Corey Cavanaugh,[1,7] Janet Tate,[6] Ying Wang,[1] Elizabeth Cross,[1] Marwin Groener,[1] Nathan Chai,[1] Zhen Wang,[1] Amy Justice,[1,6] Zhenhai Zhang,[3,4,5] Chirag R. Parikh,[8] Francis P. Wilson,[1,7] and Shuta Ishibe[1]

[1]Department of Internal Medicine, and [2]Yale School of Public Health, Department of Biostatistics, Yale Center for Analytical Sciences, Yale University School of Medicine, New Haven, Connecticut, USA. [3]State Key Laboratory of Organ Failure Research, Nanfang Hospital, [4]Department of Cardiology, Nanfang Hospital, and [5]Center for Bioinformatics, School of Basic Medical Sciences, Southern Medical University, Guangzhou, Guangdong, China. [6]VA Connecticut Healthcare System, West Haven, Connecticut, USA. [7]Program of Applied Translational Research, Yale University School of Medicine, New Haven, Connecticut, USA. [8]Department of Internal Medicine, Division of Nephrology, Johns Hopkins University, Baltimore, Maryland, USA.

We identified 2 genes, histone deacetylase 1 (*HDAC1*) and *HDAC2*, contributing to the pathogenesis of proteinuric kidney diseases, the leading cause of end-stage kidney disease. mRNA expression profiling from proteinuric mouse glomeruli was linked to Connectivity Map databases, identifying *HDAC1* and *HDAC2* with the differentially expressed gene set reversible by HDAC inhibitors. In numerous progressive glomerular disease models, treatment with valproic acid (a class I HDAC inhibitor) or SAHA (a pan-HDAC inhibitor) mitigated the degree of proteinuria and glomerulosclerosis, leading to a striking increase in survival. Podocyte HDAC1 and HDAC2 activities were increased in mice podocytopathy models, and podocyte-associated *Hdac1* and *Hdac2* genetic ablation improved proteinuria and glomerulosclerosis. Podocyte early growth response 1 (EGR1) was increased in proteinuric patients and mice in an HDAC1- and HDAC2-dependent manner. Loss of EGR1 in mice reduced proteinuria and glomerulosclerosis. Longitudinal analysis of the multicenter Veterans Aging Cohort Study demonstrated a 30% reduction in mean annual loss of estimated glomerular filtration rate, and this effect was more pronounced in proteinuric patients receiving valproic acid. These results strongly suggest that inhibition of HDAC1 and HDAC2 activities may suppress the progression of human proteinuric kidney diseases through the regulation of EGR1.

Introduction

The kidney filtration barrier is composed of fenestrated endothelial cells, the glomerular basement membrane, and the podocytes. The podocyte is a terminally differentiated epithelial cell, which in concert with the rest of the filtration barrier filters solutes while retaining large–molecular weight proteins in circulation (1, 2). Loss of kidney filtration barrier integrity results in the escape of proteins into the urine, accounting for approximately 80% of all chronic kidney disease (CKD) that afflicts over 500 million patients worldwide (3). Despite this, over 20 years have passed since the identification of novel therapeutic targets to impact the chronic course of proteinuric kidney diseases. Inhibition of the renin-angiotensin-aldosterone axis has remained the standard of care for patients, but as the incidence and prevalence of CKD and end-stage kidney disease (ESKD) continue to rise, alternative therapies are paramount to temper the progression of proteinuric kidney diseases (4, 5).

To identify novel pharmacological targets through mRNA profiling, Connectivity Map databases have been developed using cancer cell lines to provide gene signature–based drug candidates (6, 7). More recently, systems pharmacology has shown the potential use of histone deacetylase inhibitors combined with angiotensin-converting enzyme inhibitors to promote a kidney protective effect (8). Histone acetylation is governed by 2 enzymes, the histone acetyltransferases (HATs) and the histone deacetylases (HDACs), which orchestrate the addition or removal of an acetyl group on the ε amino groups of lysine residues on the histone tail (9–11). In general, the acetylation by HAT is thought to counteract the histone's positive charge, resulting in relaxation of the chromatin structure and allowing for increased access for transcription factors to modulate their target genes. Conversely, in the presence of an HDAC, histone deacetylation preferentially suppresses transcriptional activity (9, 12). HAT and HDAC also modulate acetyl groups on nonhistone proteins, altering their stability and biological function (13, 14). Within the mammalian HDAC superfamily, in the genome, there are 11 proteins that are divided into 4 families (classes I, IIa, IIb, and IV), excluding sirtuins (class III), which uniquely require NAD^+ as a cofactor for deacetylation (15, 16). Accumulating evidence suggests that the ubiquitously expressed class I HDACs, HDAC1 and HDAC2, are important during not only tissue development but the progression of diseases, such as cardiac hypertrophy, stroke, and Parkinson disease (17–19).

In this study, an unbiased gene profiling of glomeruli isolated from proteinuric mice revealed novel molecular "footprints" dysregulated in proteinuric diseases. Using a computational systems biology database, we observed that the differential expression of

Conflict of interest: The authors have declared that no conflict of interest exists.

Submitted: August 6, 2018; **Accepted:** January 10, 2019.
Reference information: *J Clin Invest*. 2019;129(3):1295–1313.
https://doi.org/10.1172/JCI124030.

genes in microarrays from glomeruli of proteinuric mice could be influenced by increased HDAC1 and HDAC2 activity, and potentially reversed by HDAC inhibitors. To test the potential effect of HDAC inhibitors, either of the FDA-approved drugs valproic acid (VPA) and suberanilohydroxamic acid (SAHA) was administered in different genetic and glomerular injury models. Administration of these drugs alleviated the degree of proteinuria and reduced progression to glomerulosclerosis. We further observed that mice lacking podocyte-associated HDAC1 and HDAC2 were resistant to progressive glomerulosclerosis, suggesting that one potential site where HDAC inhibition exerts its beneficial effect is at the podocytes. To provide further support for the hypothesis that HDAC inhibition might be an effective strategy for the treatment of kidney disease in humans, we examined data from over 120,000 veterans participating in the Veterans Aging Cohort Study, and found a strong protective effect of VPA exposure on the decline of estimated glomerular filtration rate over time, which was most pronounced in proteinuric kidney patients. These findings were not observed with VPA comparator drugs, lamotrigine, carbamazepine, or levetiracetam, which do not inhibit HDAC activity. Collectively these results reveal a potential role of HDAC inhibitors in the therapeutic armamentarium for progressive human proteinuric kidney diseases.

Results

Bioinformatics analysis suggests that HDAC1 and HDAC2 inhibition can reverse differential gene expression in mouse glomeruli isolated from a proteinuric kidney disease model. First, we sought to generate an adult-onset mouse model of severe progressive proteinuric kidney failure, as toxin-induced models such as nephrotoxic serum (NTS), lipopolysaccharide (LPS), and adriamycin induce modest proteinuria and are often self-limited (20). Therefore, we generated an adult genetic mouse model of proteinuric kidney disease by ablating *Tln1* in podocytes in a conditional doxycycline-inducible manner that was confirmed by the absence of podocyte-specific immunoreactivity (Figure 1A). Littermate mice lacking the *TetO-Cre* gene or the *Pod-rtTA* gene were used as controls. Compared with control mice, *Tln1$^{fl/fl}$ Pod-rtTA TetO-Cre* mice developed albuminuria (Figure 1B) and biochemical evidence of kidney failure with elevated creatinine levels (Figure 1C) 4 weeks after completion of doxycycline induction. Histological analysis of the kidneys demonstrated progressive glomerulosclerosis, dilated tubules with proteinaceous casts, and interstitial fibrosis evidenced by trichrome staining (Figure 1, D and E, quantified in G and H). Ultrastructural examination of these mutant kidneys by electron microscopy exhibited extensive podocyte foot process effacement 4 weeks after completion of induction (Figure 1F, quantified in I). At 4 weeks after completion of doxycycline induction, the *Tln1$^{fl/fl}$ Pod-rtTA TetO-Cre* mice had a reduction in podocyte number by WT1 staining (Figure 1J) and also a loss of actin stress fibers, similarly to the germline podocyte-specific *Tln1*-KO mice (data not shown) (20).

As these genetically modified mice developed podocyte loss, glomerulosclerosis, and progressive kidney failure, which is similar to progression of human glomerular diseases, we used this model to pursue differentially expressed genes following glomerular injury through RNA profiling of control and *Tln1$^{fl/fl}$ Pod-rtTA TetO-Cre* mouse glomeruli isolated 2 weeks after completion of doxycycline induction (Figure 2A). Analysis of the gene expression microarrays from all batches identified 100 upregulated and 88 downregulated genes in the *Tln1$^{fl/fl}$ Pod-rtTA TetO-Cre* mice (Figure 2B and Supplemental Table 1; supplemental material available online with this article; https://doi.org/10.1172/JCI124030DS1). To next probe for the differentially expressed genes, we used Drug Pair Seeker (DPS) (http://www.maayanlab.net/DPS/) to identify candidate pathways and drugs that could reverse the altered gene expression (6, 7). A generated Connectivity Map revealed that HDACs were among the most prominent pathways (Figure 2C), and DPS identified HDAC inhibitors as the perturbagen with potential to block these pathways (trichostatin A and VPA) (Supplemental Table 2). Two weeks after completion of doxycycline induction, glomeruli isolated from the *Tln1$^{fl/fl}$ Pod-rtTA TetO-Cre* mice revealed an increase in total HDAC activity (except for the sirtuin family) when compared with controls at the end of doxycycline induction (time zero), which further increased at 2 weeks after doxycycline completion (Figure 2D). However, no significant increase in *Hdac* mRNA expression (data not shown) or protein expression was observed (Figure 2E). Finally, specific examination of enriched podocytes isolated from *Tln1$^{fl/fl}$ Pod-rtTA TetO-Cre* mouse glomeruli revealed a striking increase in both HDAC1 and HDAC2 activity (Figure 2, F and G).

VPA treatment reduces albuminuria and progression of glomerular injury. Next, we examined whether inhibition of HDAC1 and HDAC2 with VPA would stabilize albuminuria or prevent the progression of glomerulosclerosis. VPA is an FDA-approved drug that has been in use for absence seizures since 1978 (21–23). Over the past 4 decades, observational and randomized trials have established its efficacy as an anti-epileptic, an anti-migraine, an anti-manic, and, more recently, an anti-proliferative chemotherapy adjunct (24–27). To examine the effect of VPA on glomerular injury in *Tln1$^{fl/fl}$ Pod-rtTA TetO-Cre* mice, VPA (150 μg/d) was administrated i.p. for 4 weeks following the completion of doxycycline induction — a time point at which albuminuria was already observed (Figure 3A and Figure 1B). Upon VPA treatment, urinary albumin levels plateaued and the rise of plasma creatinine was reduced (Figure 3, B and C). Histological analysis also demonstrated improved glomerulosclerosis, tubular dilation, and interstitial fibrosis in *Tln1$^{fl/fl}$ Pod-rtTA TetO-Cre* mice treated with VPA (Figure 3, D and E, quantified in G and H). Ultrastructural examination revealed reduced foot process effacement after VPA treatment in comparison with untreated mutant mice (Figure 3F, quantified in Figure 3I). Because of the compelling effect of VPA on progression of glomerulosclerosis in the *Tln1$^{fl/fl}$ Pod-rtTA TetO-Cre* mice, we administered vorinostat (SAHA; 20 mg/kg body weight) — another FDA-approved HDAC inhibitor for the treatment of cutaneous T cell lymphoma (28) — to examine whether there was a class effect with HDAC inhibitors. Similarly to treatment with VPA, treatment of the mutant mice with SAHA for 4 weeks following the completion of doxycycline induction resulted in stabilized albuminuria, mitigated the rise of serum creatinine, and inhibited glomerulosclerosis and interstitial fibrosis (Figure 4, A–E, quantified in G and H). Ultrastructural examination of podocytes after SAHA treatment also demonstrated a reduction in foot process effacement (Figure 4F, quantified in I). We next tested germline *Pod-Tln1*-KO and *Pod-Dnm*-DKO mice, which develop

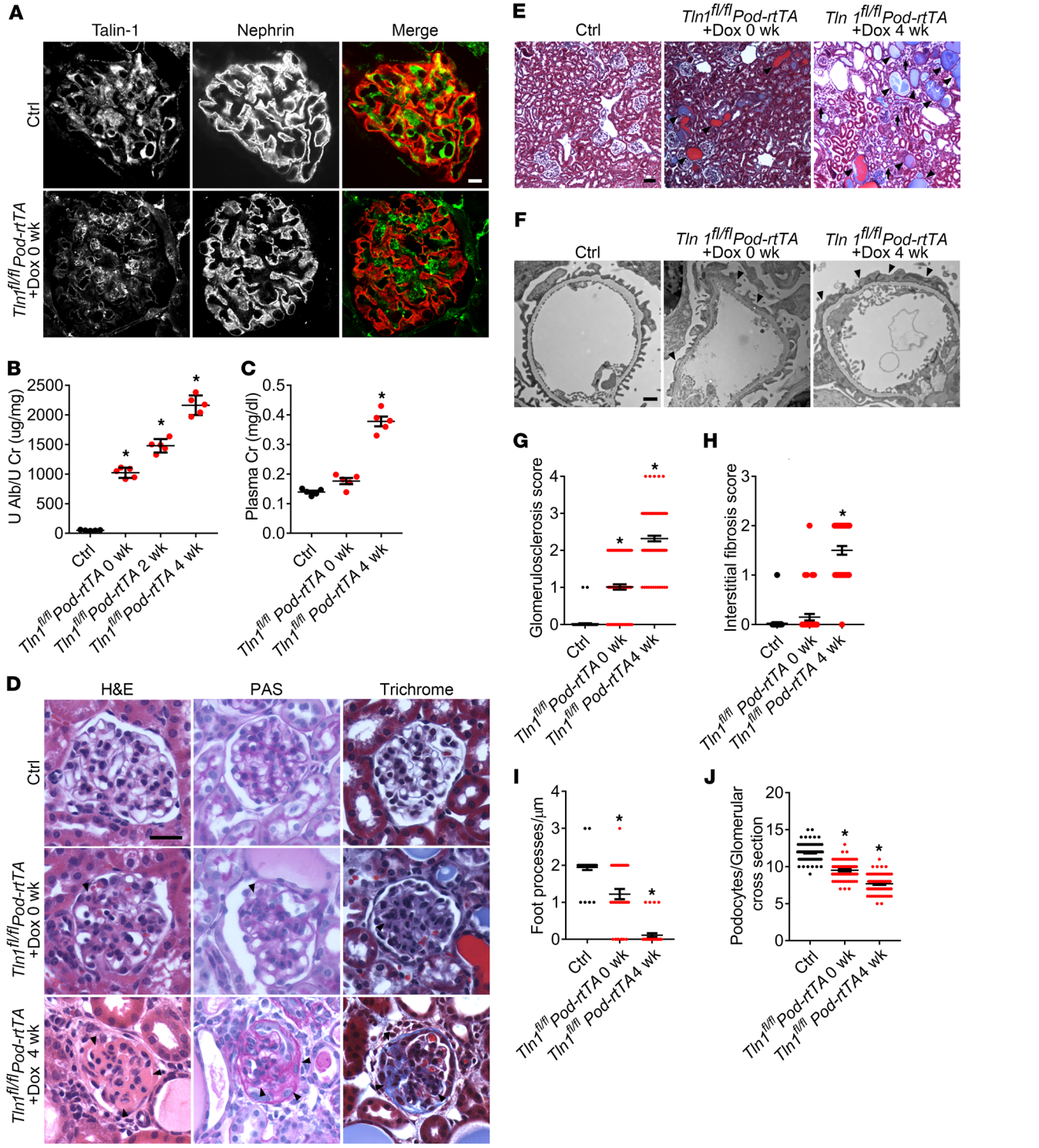

Figure 1. Doxycycline-inducible podocyte-specific *Tln1*-KO mice have massive proteinuria with kidney failure. (**A**) Representative glomerular immunofluorescence images of talin-1 (green) and nephrin (red) in doxycycline-induced (Dox-induced) control and *Tln1*$^{fl/fl}$ *Pod-rtTA TetO-Cre* mice. Scale bar: 10 μm. (**B**) Quantification of urine albumin/creatinine ratio in control and *Tln1*$^{fl/fl}$ *Pod-rtTA TetO-Cre* mice at 0, 2, and 4 weeks after completion of Dox induction. **P* < 0.05 vs. control; *n* = 5. (**C**) Plasma creatinine (Cr) levels in control and *Tln1*$^{fl/fl}$ *Pod-rtTA TetO-Cre* mice treated with Dox at 0 and 4 weeks after completion of Dox induction. **P* < 0.05 vs. control; *n* = 5. (**D**) Representative light microscope images (H&E, periodic acid–Schiff [PAS], and trichrome) of Dox-induced control and *Tln1*$^{fl/fl}$ *Pod-rtTA TetO-Cre* mouse glomeruli. Arrowheads show mesangial matrix deposition and mesangial cell proliferation. Scale bar: 25 μm. (**E**) Representative trichrome staining in control and *Tln1*$^{fl/fl}$ *Pod-rtTA TetO-Cre* mouse kidneys at representative time points. Arrowheads depict dilated tubules and proteinaceous casts, and arrows display interstitial fibrosis. Scale bar: 50 μm. (**F**) Representative transmission electron micrograph (TEM) in control and *Tln1*$^{fl/fl}$ *Pod-rtTA TetO-Cre* mouse foot processes after Dox induction. Arrowheads depict podocyte foot process effacement. Scale bar: 1 μm. (**G**) Quantification of glomerulosclerosis in **D**. **P* < 0.05 vs. control. (**H**) Quantification of interstitial fibrosis in **E**. **P* < 0.05 vs. control. (**I**) Quantification of foot processes in **F**. **P* < 0.05 vs. control. (**J**) Quantification of WT1-positive number per glomerulus in control and *Tln1*$^{fl/fl}$ *Pod-rtTA TetO-Cre* mice treated with Dox at 0 and 4 weeks after completion of Dox induction. **P* < 0.05 vs. control; *n* = 3. (**B**, **C**, and **G**–**J**) Statistically analyzed by 1-way ANOVA with Dunnett's correction.

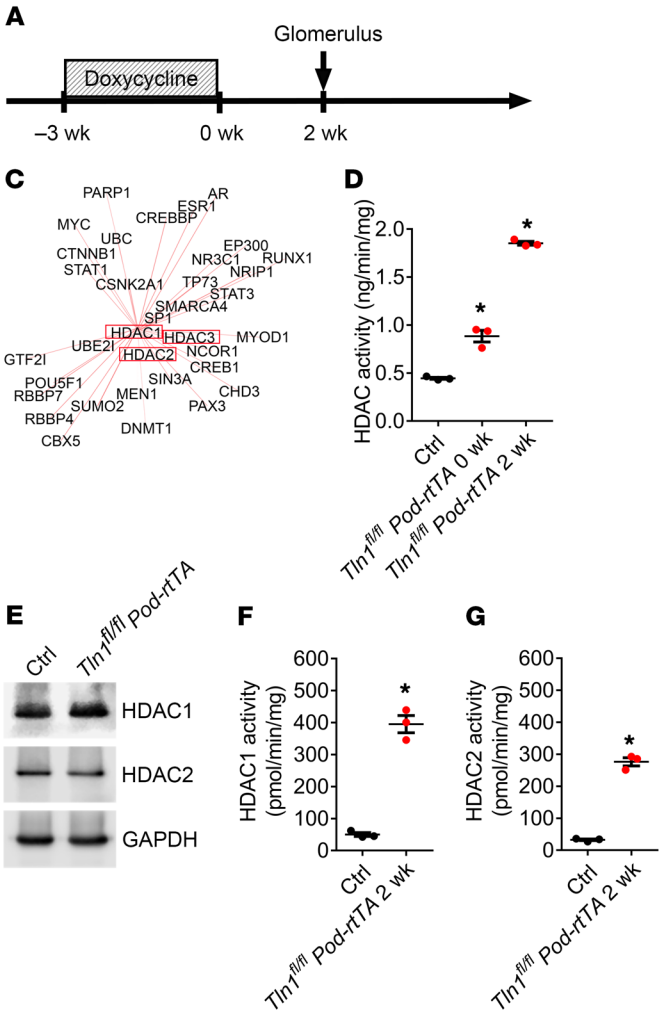

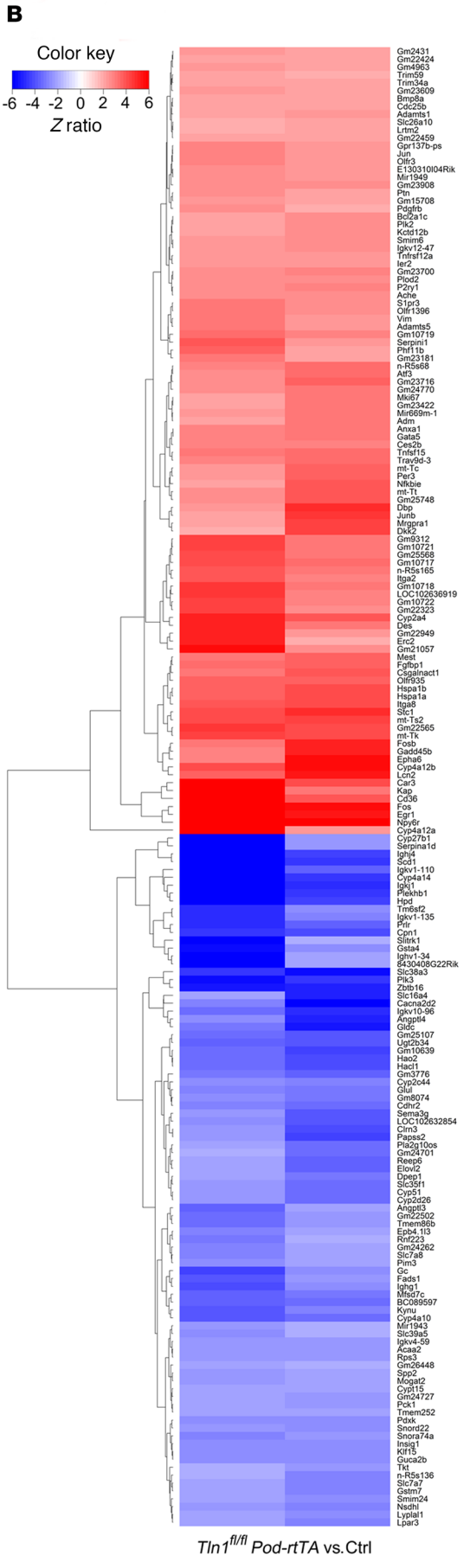

Figure 2. HDAC1 and HDAC2 are potential regulators of candidate genes analyzed by glomerular DNA microarray in Dox-induced *Tln1*$^{fl/fl}$ *Pod-rtTA TetO-Cre* mice. (**A**) Cartoon schematic of the time course of glomerular mRNA isolation for microarray in *Tln1*$^{fl/fl}$ *Pod-rtTA TetO-Cre* mice after completion of Dox induction. (**B**) Heatmap representing color-coded differentially expressed glomerular genes analyzed by *Z* ratio of *Tln1*$^{fl/fl}$ *Pod-rtTA TetO-Cre* mice to control mice 2 weeks after completion of Dox induction. (**C**) Connectivity Map analyzing the candidate genes obtained from the glomerular DNA microarray. (**D**) Total HDAC activity in control and *Tln1*$^{fl/fl}$ *Pod-rtTA TetO-Cre* mouse glomeruli 0 and 2 weeks after completion of Dox induction. *$P < 0.05$ vs. control; $n = 3$. (**E**) Representative immunoblots of HDAC1 and HDAC2 expression in control and *Tln1*$^{fl/fl}$ *Pod-rtTA TetO-Cre* mouse glomeruli. (**F** and **G**) HDAC1 (**F**) and HDAC2 (**G**) activity in control and *Tln1*$^{fl/fl}$ *Pod-rtTA TetO-Cre* mouse enriched podocytes 0 and 2 weeks after completion of Dox induction. *$P < 0.05$ vs. control; $n = 3$. (**D**) Statistically analyzed by 1-way ANOVA with Dunnett's correction. (**F** and **G**) Statistically analyzed by 2-tailed Student's *t* test.

severe albuminuria and develop histological features of focal segmental glomerulosclerosis, and interstitial damage evidenced by destroyed or dilated tubular segments (20, 29). By 6–8 weeks of age, 80%–90% of both transgenic mice died secondary to severe kidney failure. We observed robust HDAC activity in the isolated glomeruli from these 2 transgenic mice (Supplemental Figure 1A and Supplemental Figure 2A) and thus initiated VPA treatment at 2 and 3 weeks of age, respectively, time points when albuminuria was already present. VPA treatment inhibited the progression of albuminuria and glomerulosclerosis in both mutant mice while body weight was maintained (Supplemental Figure 1, B–D, and Supplemental Figure 2, B–D). Treatment of *Dnm*-DKO and *Tln1*-KO mice with VPA conferred a remarkable survival benefit, likely due to the slower progression of kidney failure (Supplemental Figure 1E and Supplemental Figure 2E). Histological analysis also displayed reduced glomerulosclerosis and interstitial fibrosis in the VPA-treated mutant mice compared with the untreated mice (Supplemental Figure 1, F and G; Supplemental Figure 2, F and G, quantified in Supplemental Figure 1, H and I; and Supplemental Figure 2, H and I). To also examine toxin-induced mouse models of podocyte injury, we treated wild-type C57BL/6 mice with rabbit anti–mouse glomerular basement membrane serum (nephrotoxic serum [NTS]) and wild-type BALB/c mice with adriamycin, which induced glomerular total HDAC activity (Supplemental Figure 3A). Treatment of these mice with VPA or SAHA reduced albuminuria and improved glomerular lesions that were provoked following NTS or adriamycin administration (Supplemental Figure 3, B–E).

Deletion of Hdac1 and Hdac2 in podocytes reduces glomerulosclerosis and interstitial fibrosis in Tln1$^{fl/fl}$ Pod-rtTA TetO-Cre mice. Because HDAC1 activity and HDAC2 activity were increased in enriched podocytes obtained from *Tln1$^{fl/fl}$ Pod-rtTA TetO-Cre* mice, and because of the beneficial effect of HDAC inhibitors in the mice, we next wanted to identify whether podocyte HDAC1 and HDAC2 activation contributes to progression of glomerular injury. As the deletion of only *Hdac1* or *Hdac2* in podocytes did not significantly improve glomerular lesions (data not shown), we tested whether loss of both HDAC1 and HDAC2 in podocytes mitigates the progression of glomerular injury. We initially confirmed that tissue-specific excision of HDAC1 and HDAC2 in the doxycycline-inducible podocyte-specific *Hdac1*- and *Hdac2*-KO mice (*Hdac1$^{fl/fl}$ Hdac2$^{fl/fl}$ Pod-rtTA TetO-Cre* mice) (Supplemental Figure 4A) displayed no kidney phenotype after completion of doxycycline induction, as demonstrated by kidney histology, urine albumin, and plasma creatinine (Supplemental Figure 4, B–E). We next examined whether podocyte-specific loss of *Hdac1* and *Hdac2* would provide protection in the *Tln1$^{fl/fl}$ Pod-rtTA TetO-Cre* mice. Four weeks after completion of doxycycline induction in the *Hdac1$^{fl/fl}$ Hdac2$^{fl/fl}$ Tln1$^{fl/fl}$ Pod-rtTA TetO-Cre* mice, we observed stable urinary albumin/creatinine ratio and markedly improved kidney function in comparison with the *Tln1$^{fl/fl}$ Pod-rtTA TetO-Cre* mice (Figure 5, A and B). Histological analysis also displayed reductions in glomerulosclerosis and interstitial fibrosis in the *Hdac1$^{fl/fl}$ Hdac2$^{fl/fl}$ Tln1$^{fl/fl}$ Pod-rtTA TetO-Cre* mice (Figure 5, C and D, quantified in F and G). Ultrastructural examination of foot processes demonstrated reduced foot process effacement in the *Hdac1$^{fl/fl}$ Hdac2$^{fl/fl}$ Tln1$^{fl/fl}$ Pod-rtTA TetO-Cre* mice (Figure 5E, quantified in H). To further validate the protective effects of *Hdac1* and *Hdac2* ablation, we examined a toxin-related podocyte injury model by injecting NTS in both control and *Hdac1$^{fl/fl}$ Hdac2$^{fl/fl}$ Pod-rtTA TetO-Cre* mice. Following NTS administration in control mice, an increase in glomerular total HDAC activity (Supplemental Figure 3A) was observed with concomitant albuminuria and glomerular injury. Markers of glomerular injury, such as albuminuria and mesangial expansion, were markedly reduced in doxycycline-induced *Hdac1$^{fl/fl}$ Hdac2$^{fl/fl}$ Pod-rtTA TetO-Cre* mice injected with NTS (Supplemental Figure 5, A and B). These data suggest that part of the striking reduction of podocyte injury and progression of glomerulosclerosis after HDAC inhibitor treatment lies at the level of the podocytes.

Increased EGR1 expression is observed in Tln1$^{fl/fl}$ Pod-rtTA TetO-Cre mice and is reversed by VPA and SAHA. Because HDAC inhibitors appear to play a critical role in maintaining the integrity of the glomerular filtration barrier following podocyte injury, we examined a microarray from glomeruli of *Tln1$^{fl/fl}$ Pod-rtTA TetO-Cre* mice with VPA in comparison with the original *Tln1$^{fl/fl}$ Pod-rtTA TetO-Cre* glomeruli microarray (Figure 6A), and identified 28 genes that were potentially reversible following VPA treatment. We confirmed by reverse transcriptase PCR the group of 28 genes that were ascertained from this second microarray (Figure 6A and Supplemental Table 3). Of these 28 genes, *Egr1*, which encodes the transcription factor early growth response 1 and has been shown to modulate the actin cytoskeleton and cell death (30–32), was detected to be the most highly upregulated gene in *Tln1$^{fl/fl}$ Pod-rtTA TetO-Cre* mouse glomeruli compared with control and also to be expressed in enriched primary podocytes (Figure 6B and Supplemental Figure 6A). We further validated that the protein expression of EGR1 was increased at the completion of doxycycline induction (time zero) (Supplemental Figure 6B) and continued at 2 weeks after doxycycline completion, which temporally correlated with increased podocyte HDAC activity. The increased EGR1 expression observed in the *Tln1$^{fl/fl}$ Pod-rtTA TetO-Cre* mouse glomerulus was mitigated in VPA- or SAHA-treated mice, or in mice lacking podocyte-associated *Hdac1* and *Hdac2* (Figure 6C, quantified in D). EGR1 expression was also increased in glomeruli isolated from *Pod-Dnm*-DKO and *Pod-Tln1*-KO mice, which was improved following VPA treatment (Supplemental Figure 6, C and D). To confirm the importance of EGR1 in human proteinuric disease, kidney biopsy samples from patients with focal segmental glomerulosclerosis demonstrated increased podocyte EGR1 expression (Figure 6E, quantified in F). Furthermore, in vitro experiments using isolated primary podocytes from *Pod-Cre Rosa-DTR^{flox}* mice treated with lipopolysaccharide (LPS) or protamine sulfate (PS), two agents that induce podocyte injury, resulted in increased HDAC activity and EGR1 expression, and the latter was reduced by VPA or SAHA (Supplemental Figure 6E; and Figure 7A, quantified in B and C). To further elucidate how EGR1 expression is regulated following podocyte injury, we examined cAMP response element–binding protein (CREB) and serum response factor (SRF), which have been previously shown to bind to the *Egr1* promoter (33). A chromatin immunoprecipitation (ChIP) assay using CREB and SRF antibodies demonstrated increased CREB binding to CRE within the *Egr1* promoter in LPS- or PS-treated primary podocytes, which was decreased by VPA or SAHA (Figure 7, D and E). SRF binding to serum response

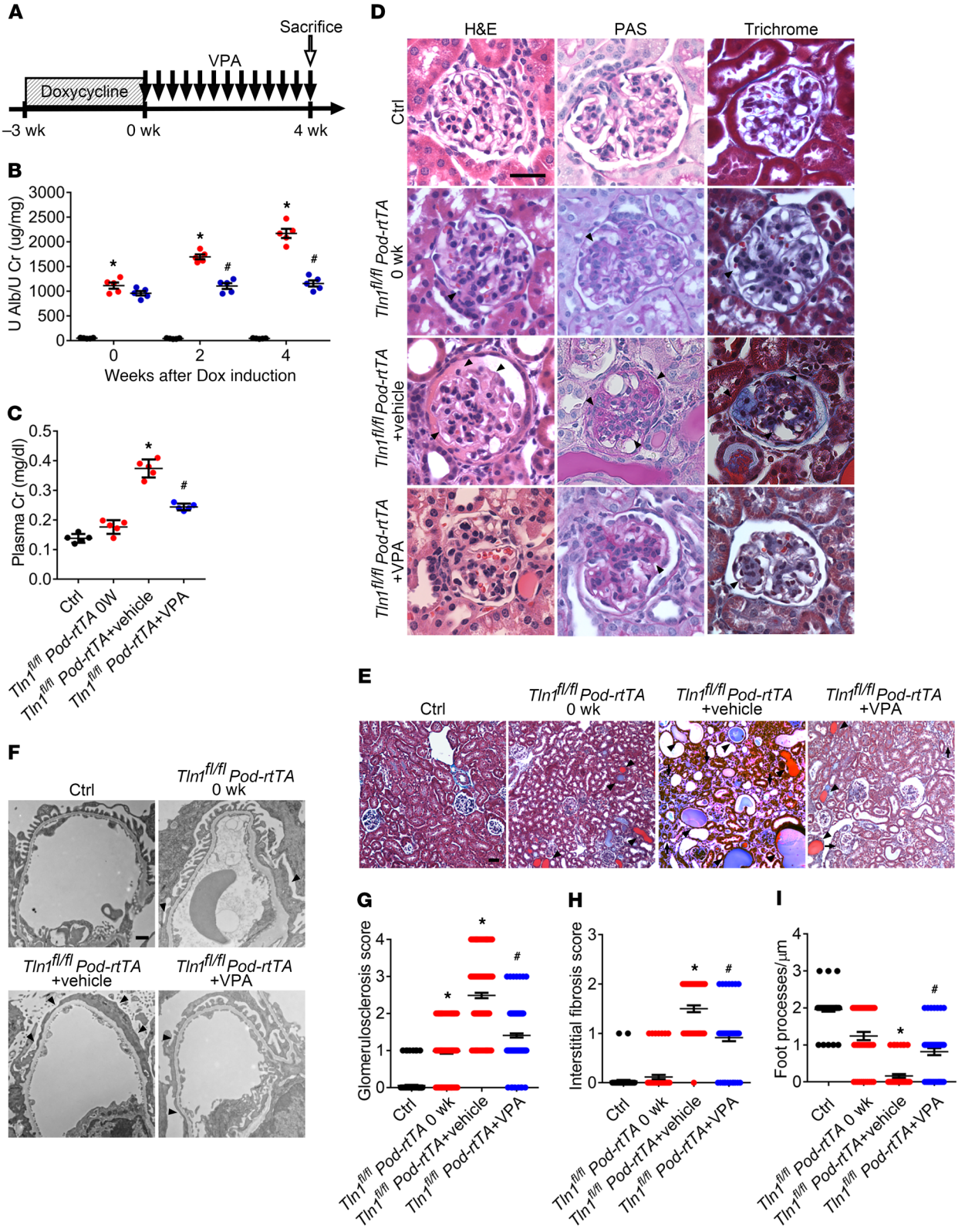
A
Sacrifice
VPA
Doxycycline
–3 wk
0 wk
4 wk
B
U Alb/U Cr (ug/mg)
Weeks after Dox induction
C
Plasma Cr (mg/dl)
Ctrl
Tln1fl/fl Pod-rtTA 0W
Tln1fl/fl Pod-rtTA+vehicle
Tln1fl/fl Pod-rtTA+VPA
D
H&E
PAS
Trichrome
Ctrl
Tln1fl/fl Pod-rtTA 0 wk
Tln1fl/fl Pod-rtTA +vehicle
Tln1fl/fl Pod-rtTA +VPA
E
Ctrl
Tln1fl/fl Pod-rtTA 0 wk
Tln1fl/fl Pod-rtTA +vehicle
Tln1fl/fl Pod-rtTA +VPA
F
Ctrl
Tln1fl/fl Pod-rtTA 0 wk
Tln1fl/fl Pod-rtTA +vehicle
Tln1fl/fl Pod-rtTA +VPA
G
Glomerulosclerosis score
H
Interstitial fibrosis score
I
Foot processes/μm

Figure 3. VPA reduces podocyte injury in Dox-inducible *Tln1*$^{fl/fl}$ *Pod-rtTA TetO-Cre* mice. (**A**) Time course schematic of Dox-induced *Tln1*$^{fl/fl}$ *Pod-rtTA TetO-Cre* mice treated with or without VPA. (**B**) Urine albumin/creatinine ratio in control (black) and *Tln1*$^{fl/fl}$ *Pod-rtTA TetO-Cre* mice treated with vehicle or VPA (red: vehicle; blue: VPA) at 0, 2, and 4 weeks following Dox induction. *$P < 0.05$ vs. control mice, #$P < 0.05$ vs. vehicle-treated *Tln1*$^{fl/fl}$ *Pod-rtTA TetO-Cre* mice; $n = 5$. (**C**) Plasma creatinine in control and *Tln1*$^{fl/fl}$ *Pod-rtTA TetO-Cre* mice treated with vehicle or VPA 0 and 4 weeks following Dox induction. *$P < 0.05$ vs. control mice, #$P < 0.05$ vs. vehicle-treated *Tln1*$^{fl/fl}$ *Pod-rtTA TetO-Cre* mice; $n = 5$. (**D**) H&E, PAS, and trichrome staining in control and *Tln1*$^{fl/fl}$ *Pod-rtTA TetO-Cre* mouse glomeruli treated with vehicle or VPA 0 or 4 weeks following Dox induction. Arrowheads show mesangial cell matrix deposition and proliferation. Scale bar: 25 μm. (**E**) Trichrome staining of control and *Tln1*$^{fl/fl}$ *Pod-rtTA TetO-Cre* mice kidneys treated with vehicle or VPA at 0 or 4 weeks following Dox induction. Arrowheads show dilated tubules and proteinaceous casts; arrows display interstitial fibrosis. Scale bar: 50 μm. (**F**) TEM in control and *Tln1*$^{fl/fl}$ *Pod-rtTA TetO-Cre* mice treated with vehicle or VPA at 0 or 4 weeks following Dox induction. Arrowheads depict podocyte foot process effacement. Scale bar: 1 μm. (**G**) Glomerulosclerosis quantification in D. *$P < 0.05$ vs. control mice, #$P < 0.05$ vs. vehicle-treated *Tln1*$^{fl/fl}$ *Pod-rtTA TetO-Cre* mice. (**H**) Interstitial fibrosis quantification in E. *$P < 0.05$ vs. control mice, #$P < 0.05$ vs. vehicle-treated *Tln1*$^{fl/fl}$ *Pod-rtTA TetO-Cre* mice. (**I**) Foot process quantification in F. *$P < 0.05$ vs. control mice, #$P < 0.05$ vs. vehicle-treated *Tln1*$^{fl/fl}$ *Pod-rtTA TetO-Cre* mice. (**B**, **C**, and **G**–**I**) Statistics using 1-way ANOVA with Dunnett's correction.

element (SRE) within the *Egr1* promoter was unchanged in LPS- or PS-treated primary podocytes (Supplemental Figure 6, F–I). Previous studies have shown that CRE binding in the target gene promoter can be increased by the phosphorylation of CREB at Ser133 residue (34). In primary podocytes treated with LPS for 3 hours or PS for 1 hour, we observed a robust increase in phosphorylated CREB (Ser133), which could be reversed by either VPA or SAHA treatment, suggesting that HDAC inhibitors may reduce CREB phosphorylation (Figure 7F, quantified in G and H).

Loss of Egr1 in Tln1$^{fl/fl}$ *Pod-rtTA TetO-Cre mice reduces progressive albuminuria and glomerulosclerosis*. To next determine the importance of EGR1 in vivo, we generated *Egr1*$^{-/-}$ *Tln1*$^{fl/fl}$ *Pod-rtTA TetO-Cre* mice, to assess whether loss of this gene could rescue the *Tln1*$^{fl/fl}$ *Pod-rtTA TetO-Cre* mice. We found a striking reduction in albuminuria, kidney failure, glomerulosclerosis, and interstitial fibrosis (Figure 8, A–D, quantified in E and F) similar to what was observed following VPA treatment. To validate the effect of EGR1 in a toxin-related podocyte injury model, *Egr1*$^{-/-}$ mice were treated with NTS. Compared with control mice, *Egr1*$^{-/-}$ mice had reduced NTS-induced albuminuria and glomerular lesions (Supplemental Figure 8, A and B). Next, to elucidate a role of EGR1 upregulation in podocyte injury, we examined F-actin staining patterns in primary podocytes and TUNEL staining in *Tln1*$^{fl/fl}$ *Pod-rtTA TetO-Cre* mice with doxycycline, as increased EGR1 expression has been shown to regulate the actin cytoskeleton and induce cell apoptosis (35–38). Loss of podocyte-associated EGR1 expression or VPA treatment resulted in stabilization and maintenance of actin stress fibers after LPS treatment (for 6 hours) and PS treatment (for 1 hour) in comparison with controls (Figure 9A, quantified in B–D; and Supplemental Figure 7A, quantified in C). Conversely, the overexpression of EGR1 in LPS- and VPA-treated control primary podocytes resulted in loss of actin stress fibers (Supplemental Figure 7B, quantified in D). Furthermore, VPA treatment ameliorated LPS-induced cell spreading (increased cell surface area), while the overexpression of EGR1 in LPS- and VPA-treated control primary podocytes resulted in increased cell spreading (Figure 9E). VPA therapy also mitigated podocyte loss in comparison with untreated doxycycline-induced *Tln1*$^{fl/fl}$ *Pod-rtTA TetO-Cre* mice (Supplemental Figure 7E). However, TUNEL staining in kidneys 2 weeks after completion of doxycycline revealed apoptotic cells (TUNEL-positive cells) in the tubular segments but not in podocytes (stained with WT1) (Supplemental Figure 7F), suggesting that VPA treatment may protect podocytes by stabilizing the actin cytoskeleton and preventing other forms of programmed cell death.

VPA treatment improves decline of estimated glomerular filtration rate in proteinuric patients. To support the hypothesis that HDAC inhibition may also be a potent therapeutic strategy against human proteinuric kidney disease, we next interrogated the Veterans Aging Cohort Study. Among 122,870 veterans participating in the Study and eligible for analysis, the median (IQR) duration of follow-up was 9.0 (4.7–13.2) years. The mean rate of decline in estimated glomerular filtration rate (eGFR) was –0.94 (standard error 0.007) ml/1.73 m^2/yr, which is consistent with several large, US population–based studies (39, 40). Veterans exposed to VPA were slightly younger than those who were not exposed. They also had higher baseline eGFR and were less likely to be infected with HIV or HCV. They were more likely to be diabetic and to have hypertension, and bore a strikingly higher rate of psychiatric comorbidities, with fully 76.5% of those in the VPA group carrying a diagnosis of bipolar disorder compared with 21.4% of those in the unexposed group (Supplemental Table 4). Exposure to VPA ($n = 2269$) was associated with a significantly attenuated rate of decline in eGFR, with an unadjusted mean annual change in eGFR of –0.61 (0.07) ml/1.73 m^2/yr among those who received VPA compared with –0.94 (0.007) ml/1.73 m^2/yr among those who did not receive the agent — a 35% reduction in the rate of decline. The fully adjusted difference was 0.16 (0.07) ml/min/1.73 m^2/yr, $P = 0.02$ (Figure 10A). Within-patient analyses (restricted to patients who initiated VPA while under observation) revealed that, before initiation of VPA, the average decline in eGFR was –0.93 (standard error 0.05) ml/1.73 m^2/yr compared with –0.32 (standard error 0.09) ml/1.73 m^2/yr after the initiation of VPA ($P < 0.0001$) (Figure 10B).

Next, we analyzed the patients stratified by proteinuria. Among the patients with no or mild proteinuria (1+ or less on urine dipstick), the unadjusted mean yearly decline in eGFR was –0.92 (0.007) ml/1.73 m^2/yr in the patients not receiving VPA, compared with –0.61 (0.07) ml/1.73 m^2/yr in those receiving VPA (Figure 10C). In the patients with heavy proteinuria (2+ or more on urine dipstick), the unadjusted mean yearly decline in eGFR was –2.5 (0.05) ml/1.73 m^2/yr in patients not receiving VPA, compared with –0.56 (0.66) ml/1.73 m^2/yr in those receiving VPA (Figure 10D). After full adjustment, this effect modification by proteinuria was statistically significant at $P = 0.02$, suggesting that the beneficial effect of VPA is more pronounced in patients with worse proteinuria.

These results were robust to multiple sensitivity analyses. After exclusion of all patients who ever received lithium (a known nephrotoxic agent that is used for similar indications to VPA in this population), the protective effect of VPA and the interaction between VPA benefit and proteinuria were maintained

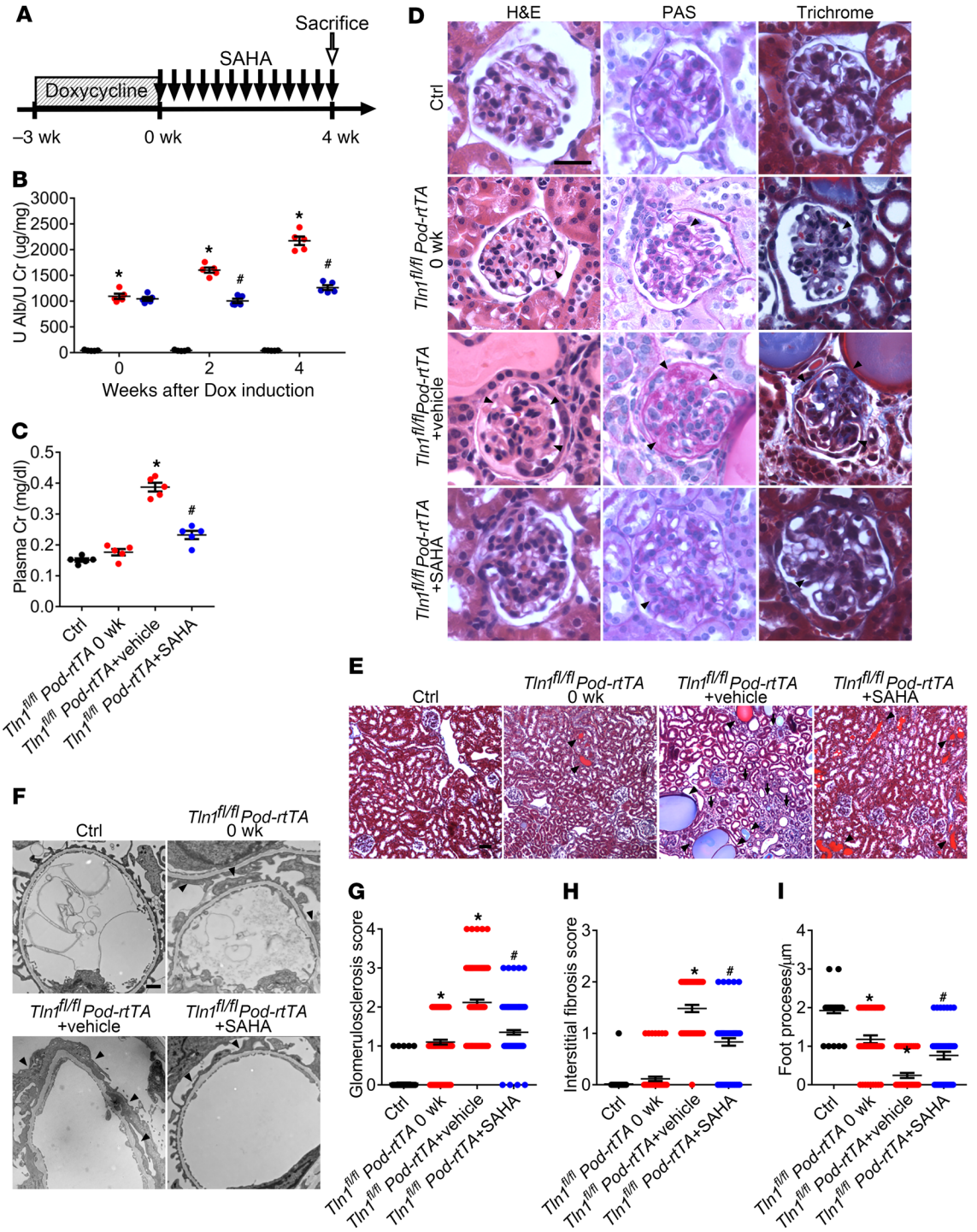

Figure 4. SAHA reduces podocyte injury in Dox-inducible *Tln1*$^{fl/fl}$ *Pod-rtTA TetO-Cre* mice. (**A**) Time course schematic of Dox-induced *Tln1*$^{fl/fl}$ *Pod-rtTA TetO-Cre* mice with or without SAHA. (**B**) Urine albumin/creatinine ratio in control (black) and *Tln1*$^{fl/fl}$ *Pod-rtTA TetO-Cre* mice with vehicle or SAHA (red: +vehicle; blue: +SAHA) 0, 2, and 4 weeks following Dox induction. *$P < 0.05$ vs. control mice, #$P < 0.05$ vs. vehicle-treated *Tln1*$^{fl/fl}$ *Pod-rtTA TetO-Cre* mice; $n = 5$. (**C**) Plasma creatinine in control and *Tln1*$^{fl/fl}$ *Pod-rtTA TetO-Cre* mice treated with vehicle or SAHA at 0 and 4 weeks following Dox induction. *$P < 0.05$ vs. control mice, #$P < 0.05$ vs. vehicle-treated *Tln1*$^{fl/fl}$ *Pod-rtTA TetO-Cre* mice; $n = 5$. (**D**) H&E, PAS, and trichrome staining in control and *Tln1*$^{fl/fl}$ *Pod-rtTA TetO-Cre* mouse glomeruli treated with vehicle or SAHA at 0 and 4 weeks following Dox induction. Arrowheads show mesangial cell matrix deposition and proliferation. Scale bar: 25 μm. (**E**) Trichrome staining of control and *Tln1*$^{fl/fl}$ *Pod-rtTA TetO-Cre* mouse kidneys treated with vehicle or SAHA at 0 and 4 weeks following Dox induction. Arrowheads show dilated tubules and proteinaceous casts; arrows display interstitial fibrosis. Scale bar: 50 μm. (**F**) TEM in control and *Tln1*$^{fl/fl}$ *Pod-rtTA TetO-Cre* mice treated with vehicle or SAHA at 0 and 4 weeks following Dox induction. Arrowheads depict podocyte foot process effacement. Scale bar: 1 μm. (**G**) Glomerulosclerosis quantification in **D**. *$P < 0.05$ vs. control mice, #$P < 0.05$ vs. vehicle-treated *Tln1*$^{fl/fl}$ *Pod-rtTA TetO-Cre* mice. (**H**) Interstitial fibrosis quantification in **E**. *$P < 0.05$ vs. control mice, #$P < 0.05$ vs. vehicle-treated *Tln1*$^{fl/fl}$ *Pod-rtTA TetO-Cre* mice. (**I**) Foot process quantification in **F**. *$P < 0.05$ vs. control mice, #$P < 0.05$ vs. vehicle-treated *Tln1*$^{fl/fl}$ *Pod-rtTA TetO-Cre* mice. (**B**, **C**, and **G**–**I**) Statistics using 1-way ANOVA with Dunnett's correction.

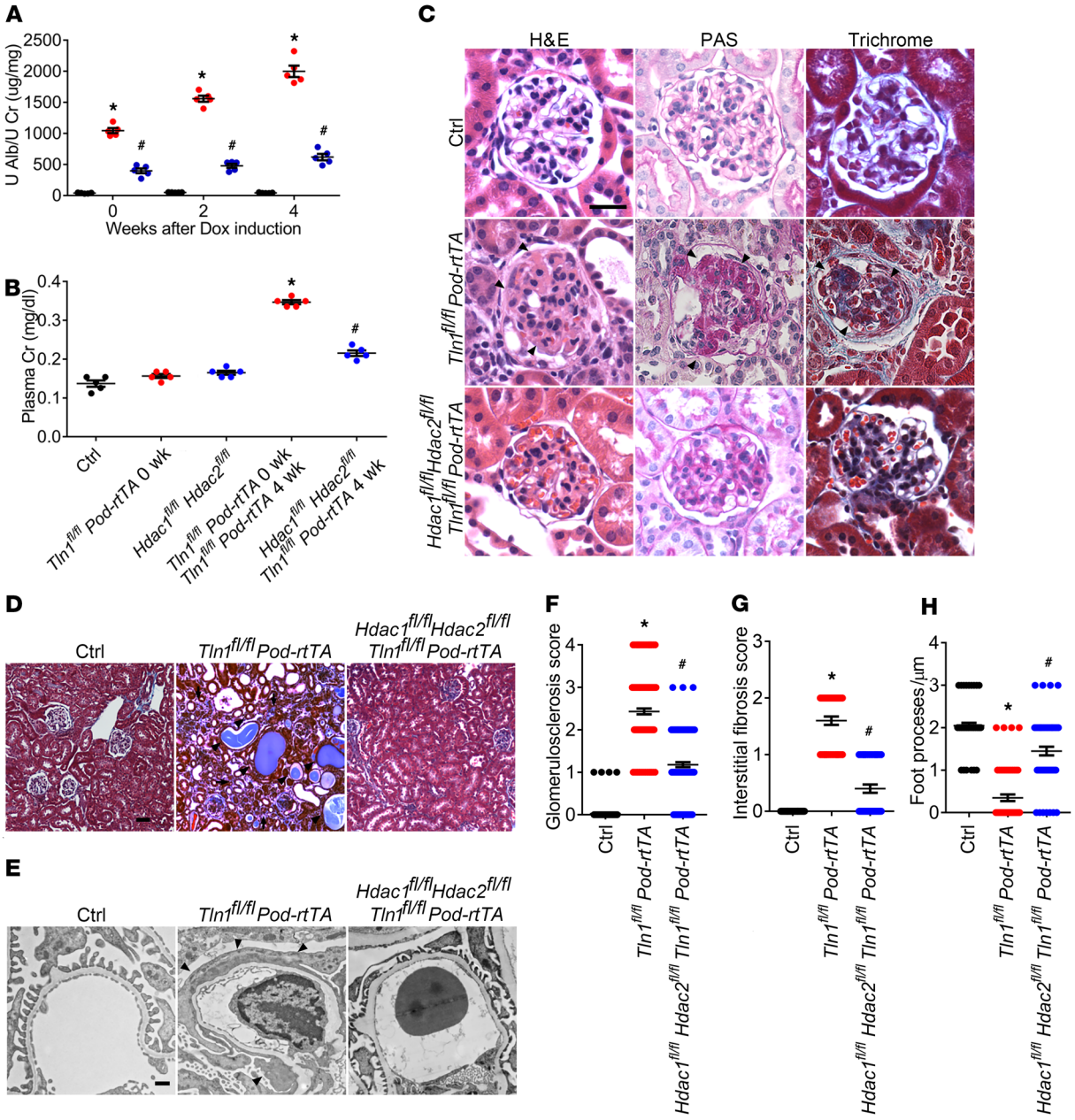

Figure 5. Podocyte deletion of *Hdac1* and *Hdac2* improves glomerulosclerosis and kidney failure in *Tln1*$^{fl/fl}$ *Pod-rtTA TetO-Cre* mice induced with Dox. (**A**) Quantification of urine albumin/creatinine ratio in control (black), *Tln1*$^{fl/fl}$ *Pod-rtTA TetO-Cre* (red), and *Hdac1*$^{fl/fl}$ *Hdac2*$^{fl/fl}$ *Tln1*$^{fl/fl}$ *Pod-rtTA TetO-Cre* (blue) mice at 0, 2, and 4 weeks after completion of Dox induction. **P* < 0.05 vs. control mice, $^{\#}$*P* < 0.05 vs. *Tln1*$^{fl/fl}$ *Pod-rtTA TetO-Cre* mice; *n* = 5. (**B**) Plasma creatinine in control, *Tln1*$^{fl/fl}$ *Pod-rtTA TetO-Cre*, and *Hdac1*$^{fl/fl}$ *Hdac2*$^{fl/fl}$ *Tln1*$^{fl/fl}$ *Pod-rtTA TetO-Cre* mice after completion of Dox induction. **P* < 0.05 vs. control mice, $^{\#}$*P* < 0.05 vs. *Tln1*$^{fl/fl}$ *Pod-rtTA TetO-Cre* mice; *n* = 5. (**C**) Representative light microscopy images (H&E, PAS, and trichrome) of control, *Tln1*$^{fl/fl}$ *Pod-rtTA TetO-Cre*, and *Hdac1*$^{fl/fl}$ *Hdac2*$^{fl/fl}$ *Tln1*$^{fl/fl}$ *Pod-rtTA TetO-Cre* mouse glomeruli 4 weeks after completion of Dox induction. Arrowheads show mesangial matrix deposition and mesangial cell proliferation. Scale bar: 25 μm. (**D**) Representative trichrome staining in control, *Tln1*$^{fl/fl}$ *Pod-rtTA TetO-Cre*, and *Hdac1*$^{fl/fl}$ *Hdac2*$^{fl/fl}$ *Tln1*$^{fl/fl}$ *Pod-rtTA TetO-Cre* mouse kidneys 4 weeks after completion of Dox induction. Arrowheads show dilated tubules and proteinaceous casts; arrows display interstitial fibrosis. Scale bar: 50 μm. (**E**) Representative TEM in control, *Tln1*$^{fl/fl}$ *Pod-rtTA TetO-Cre*, and *Hdac1*$^{fl/fl}$ *Hdac2*$^{fl/fl}$ *Tln1*$^{fl/fl}$ *Pod-rtTA TetO-Cre* mouse kidneys 4 weeks after completion of Dox induction. Arrowheads depict podocyte foot process effacement. Scale bar: 1 μm. (**F**) Quantification of glomerulosclerosis in **C**. **P* < 0.05 vs. control mice, $^{\#}$*P* < 0.05 vs. *Tln1*$^{fl/fl}$ *Pod-rtTA TetO-Cre* mice. (**G**) Quantification of interstitial fibrosis in **D**. **P* < 0.05 vs. control mice, $^{\#}$*P* < 0.05 vs. *Tln1*$^{fl/fl}$ *Pod-rtTA TetO-Cre* mice. (**H**) Quantification of foot processes in **E**. **P* < 0.05 vs. control mice, $^{\#}$*P* < 0.05 vs. *Tln1*$^{fl/fl}$ *Pod-rtTA TetO-Cre* mice. (**A**, **B**, and **F**–**H**) Statistically analyzed by 1-way ANOVA with Dunnett's correction.

(*P* = 0.008 and *P* = 0.07, respectively). Analyses that examined the effects of the comparator agents lamotrigine, carbamazepine, and levetiracetam revealed no protection of eGFR associated with exposure (Figure 11, A–D).

Discussion

For the last 20 years, the mainstay of treatment of proteinuric kidney diseases that often lead to CKD has been to block the renin-angiotensin axis (41). However, various kinds of renin-

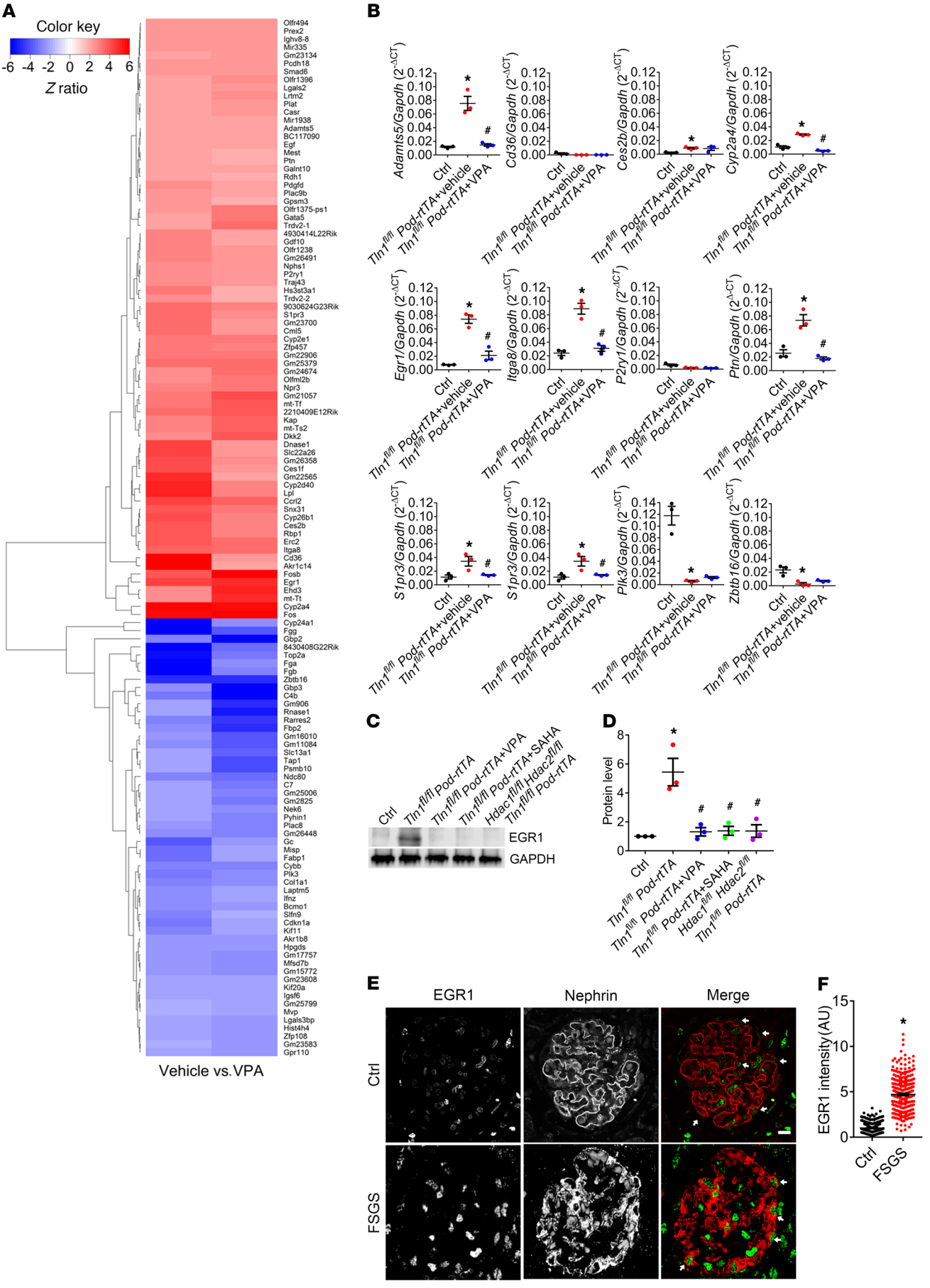
A
Color key
-6 -4 -2 0 2 4 6
Z ratio
Vehicle vs. VPA
B
Adamts5/Gapdh (2^-ΔCT)
Cd36/Gapdh (2^-ΔCT)
Ces2b/Gapdh (2^-ΔCT)
Cyp2a4/Gapdh (2^-ΔCT)
Egr1/Gapdh (2^-ΔCT)
Itga8/Gapdh (2^-ΔCT)
P2ry1/Gapdh (2^-ΔCT)
Ptn/Gapdh (2^-ΔCT)
S1pr3/Gapdh (2^-ΔCT)
S1pr3/Gapdh (2^-ΔCT)
Plk3/Gapdh (2^-ΔCT)
Zbtb16/Gapdh (2^-ΔCT)
Ctrl
Tln1fl/fl Pod-rtTA+vehicle
Tln1fl/fl Pod-rtTA+VPA
C
Ctrl
Tln1fl/fl Pod-rtTA
Tln1fl/fl Pod-rtTA+VPA
Tln1fl/fl Pod-rtTA+SAHA
Hdac1fl/fl Hdac2fl/fl
Tln1fl/fl Pod-rtTA
EGR1
GAPDH
D
Protein level
Tln1fl/fl Hdac2fl/fl
E
EGR1
Nephrin
Merge
Ctrl
FSGS
F
EGR1 intensity (AU)
Ctrl
FSGS

Figure 6. VPA treatment mitigates CREB-mediated EGR1 upregulation in *Tln1*$^{fl/fl}$ *Pod-rtTA TetO-Cre* mouse glomeruli. (**A**) Heatmap representing color-coded differential glomerular genes analyzed by *Z* ratio of *Tln1*$^{fl/fl}$ *Pod-rtTA TetO-Cre* mice with vehicle to those with VPA, 2 weeks after completion of Dox induction. (**B**) Reverse transcriptase PCR of the candidate genes in control, and *Tln1*$^{fl/fl}$ *Pod-rtTA TetO-Cre* mice treated or not treated with VPA 2 weeks after completion of Dox induction. *$P < 0.05$ vs. control mice, $^{\#}P < 0.05$ vs. *Tln1*$^{fl/fl}$ *Pod-rtTA TetO-Cre* mice; $n = 3$. (**C**) Representative immunoblots of EGR1 and GAPDH in glomeruli of control mice, *Tln1*$^{fl/fl}$ *Pod-rtTA TetO-Cre* mice treated or not treated with VPA or SAHA, and *Hdac1*$^{fl/fl}$ *Hdac2*$^{fl/fl}$ *Tln1*$^{fl/fl}$ *Pod-rtTA TetO-Cre* mice. (**D**) Quantification of EGR1 immunoblots in **C**. *$P < 0.05$ vs. control mice, $^{\#}P < 0.05$ vs. *Tln1*$^{fl/fl}$ *Pod-rtTA TetO-Cre* mice; $n = 3$. (**E**) Representative immunofluorescence images of EGR1 (green) and nephrin (red) in control and focal segmental glomerulosclerosis (FSGS) patient glomeruli. Arrows display podocyte EGR1 staining. Scale bar: 20 μm. (**F**) Quantification of podocyte EGR1 immunofluorescence intensity in **E**. *$P < 0.05$ vs. control; $n = 3$. (**B** and **D**) Statistically analyzed by 1-way ANOVA with Dunnett's correction. (**F**) Statistically analyzed by 2-tailed Student's *t* test.

angiotensin system inhibitors have been shown to have only a marginal beneficial effect on progression of proteinuria and CKD. The increasing global prevalence of ESKD indicates the need for novel therapies for proteinuric kidney diseases (4, 42). Therefore, in this study, we aimed to uncover novel molecular pathways that are potential targets for therapeutic intervention. From our unbiased screen using microarray data from injured mouse glomeruli, we identified phosphorylated-CREB–induced upregulation of EGR1 that may be governed by increased HDAC1 and HDAC2 activation resulting in foot process effacement. Inhibition by HDAC inhibitors protected podocytes and mitigated the progression and damage of the glomerular filtration barrier (Figure 12).

VPA is a common oral medication that has been in existence for close to 40 years, for the treatment of neurologic and psychiatric diseases (43). Our initial decision to pursue VPA following our bioinformatics analysis was based on the drug's favorable side effect profile in relation to the stigmata of ESKD, which is a critical attribute in entertaining treatment options. Treatment with VPA, a class I HDAC inhibitor, as well as SAHA, an FDA-approved pan-HDAC inhibitor, strikingly improved both the progression of kidney disease, and VPA treatment improved the lifespan in 2 lines of transgenic mice that died as a result of kidney failure. Previous studies have shown that HDACs promote progression of glomerular disease as well as kidney fibrosis through the TGF-β signaling pathway (44–46). It has been shown that HDAC inhibitors improve adriamycin-induced glomerular injury through downregulation of profibrotic and inflammatory genes (47), and combinations of HDAC inhibitor and renin-angiotensin system inhibitors improve kidney function in an HIV-associated glomerular injury model (8). However, HDAC inhibitors' sites of action have remained elusive. Through our study, we speculate that inhibition of HDAC1 and HDAC2 activity specifically in podocytes is critical, as genetic ablation of *Hdac1* and *Hdac2* strikingly mitigated the progression of albuminuria and glomerulosclerosis. Deletion of either podocyte *Hdac1* or *Hdac2* alone did not significantly improve proteinuria or kidney failure in *Tln1*$^{fl/fl}$ *Pod-rtTA TetO-Cre* mice. This lack of improvement is likely due to the redundant and compensatory roles of HDAC1 and HDAC2, as previous studies have shown that knockdown or deletion of either *Hdac1* or *Hdac2* alone is not sufficient to block histone acetylation (48, 49). Other investigators have also shown that following podocyte injury, HDAC4 and HDAC9 expression is increased, inhibiting autophagy, and reducing nephrin and podocin expression, respectively (50, 51). Therefore, further studies examining each HDAC protein and the relationship between HDAC families in the pathogenesis of glomerular disease progression are required.

Through our microarray analysis, we also determined that one of the likely targets regulated by HDAC1 and HDAC2 is a transcription factor, EGR1. Genetic loss of *Egr1* on a *Tln1*$^{fl/fl}$ *Pod-rtTA TetO-Cre* mouse background also reduced albuminuria and the progression of kidney disease, mimicking what was observed when these mice were treated with VPA. EGR1, one of the immediate-early response genes, was upregulated following several stimuli, such as growth factors and oxygen deprivation (52–54). Several studies have demonstrated that EGR1 upregulation induces mesangial cell proliferation, kidney interstitial fibrosis through the TGF-β signaling pathway, and cellular apoptosis in cancer cells (55–59). EGR1 upregulation may also be important for progression of glomerular disease not only in podocytes but also in other cell types. Interestingly, HDAC inhibitors have been shown to activate EGR1 in other cell types, suggesting cell-specific differences in regulation. These findings motivate further analysis to understand the role of EGR1 expression in the progression of glomerular diseases by use of cell-specific conditional *Egr1*-knockout mice (60–62).

In our results, HDAC inhibitors decreased CREB phosphorylation induced by LPS or PS in control podocytes, which resulted in reduced CREB binding to *Egr1* promoter. It has been shown that kinases such as PKA, PKC, CaMK, ERK, AKT, and PTEN can regulate CREB phosphorylation (63–68). Previous studies also revealed that HDAC inhibitors increase PTEN expression in 293T cells (69), but further studies will be needed to elucidate the link between PTEN and CREB phosphorylation following HDAC inhibition.

Lastly, a strong benefit of VPA in reducing loss of eGFR was demonstrated in a large longitudinal cohort of patients taking this medication for nonrenal indications. The findings were particularly robust in patients with proteinuria, in whom VPA administration was associated with significantly preserved kidney function over many years. Though observational data are subject to confounding by indication, these results are strengthened by the fact that VPA is not used in the management of kidney disease nor is the medication dose-adjusted among those with worse kidney function. Though our observational results were consistent across multiple subanalyses and sensitivity analyses, observational data cannot infer causation, and residual confounding may explain some of the observed effects. However, the lack of effect seen in analyses of non–HDAC inhibitor comparator agents may attenuate this concern. In addition, the Veterans Aging Cohort Study is predominantly male, limiting generalizability of these findings to other populations, while some patients may have obtained medications outside the Veterans Affairs system, which may lead to misclassification bias. Yet this would tend to bias our results toward the null.

In conclusion, we establish that HDAC1 and HDAC2 activation plays an important role in progression of glomerular disease through EGR1 upregulation. Treatment with VPA not only improved kidney function in proteinuric mice, but also ameliorated

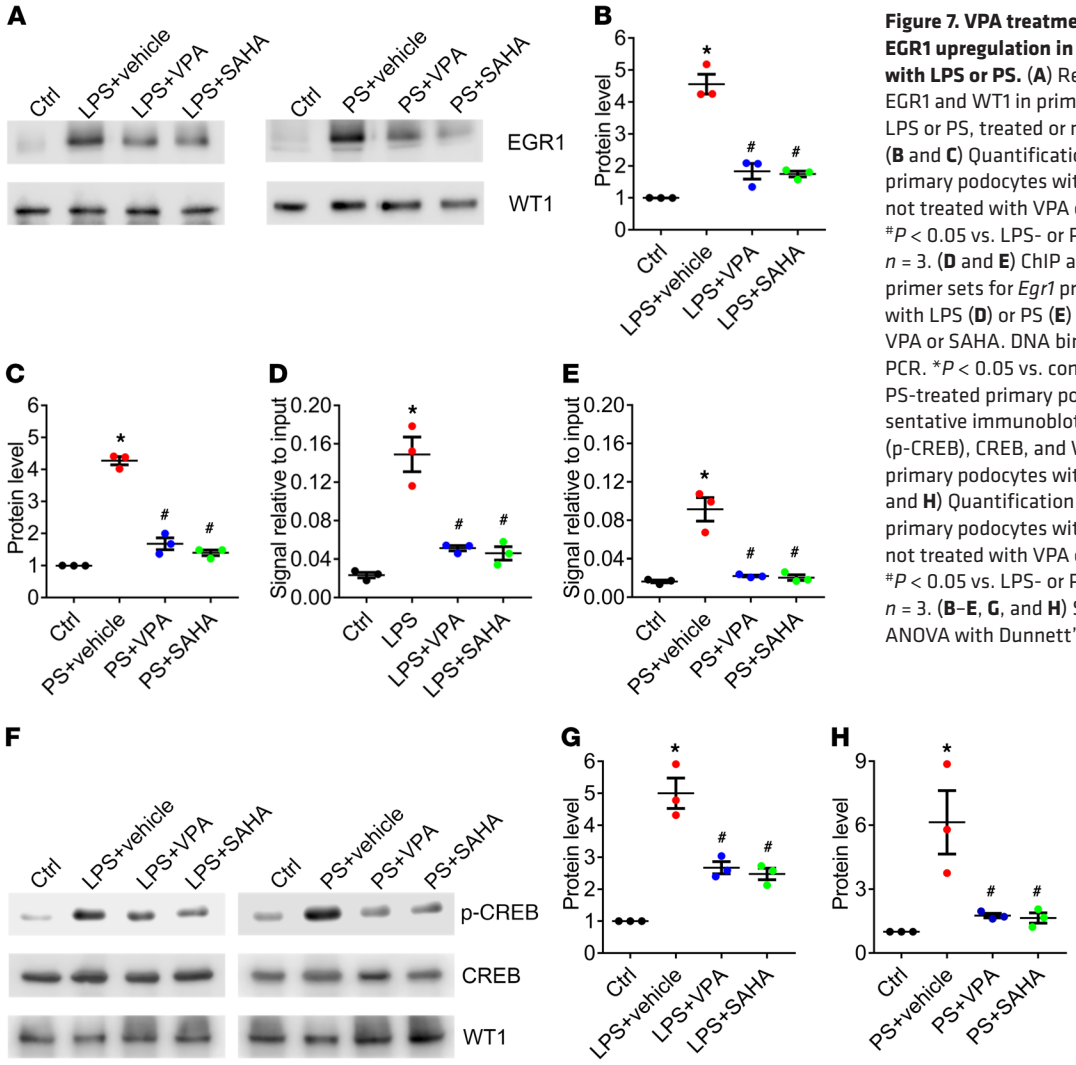

Figure 7. VPA treatment mitigates CREB-mediated EGR1 upregulation in primary podocytes treated with LPS or PS. (**A**) Representative immunoblots of EGR1 and WT1 in primary podocytes with or without LPS or PS, treated or not treated with VPA or SAHA. (**B** and **C**) Quantification of EGR1 immunoblots in primary podocytes with LPS (**B**) or PS (**C**) treated or not treated with VPA or SAHA. $^{*}P < 0.05$ vs. control, $^{\#}P < 0.05$ vs. LPS- or PS-treated primary podocytes; $n = 3$. (**D** and **E**) ChIP assay using CREB antibody and primer sets for *Egr1* promoter in primary podocytes with LPS (**D**) or PS (**E**) treated or not treated with VPA or SAHA. DNA binding was determined by PCR. $^{*}P < 0.05$ vs. control, $^{\#}P < 0.05$ vs. LPS- or PS-treated primary podocytes; $n = 3$. (**F**) Representative immunoblots of phosphorylated CREB (p-CREB), CREB, and WT1 in LPS- or PS-treated primary podocytes with or without VPA or SAHA. (**G** and **H**) Quantification of p-CREB immunoblots in primary podocytes with LPS (**G**) or PS (**H**) treated or not treated with VPA or SAHA. $^{*}P < 0.05$ vs. control, $^{\#}P < 0.05$ vs. LPS- or PS-treated primary podocytes; $n = 3$. (**B**–**E**, **G**, and **H**) Statistically analyzed by 1-way ANOVA with Dunnett's correction.

eGFR decline in proteinuric kidney disease patients. This provides compelling evidence for whether progression of proteinuric kidney diseases can be altered using VPA in a prospective manner and further motivates studies for drug repurposing of this class of agents for successful treatment of human progressive proteinuric kidney diseases in the not so distant future.

Methods

Antibodies and plasmid. Mouse anti–Wilms tumor 1 (anti-WT1) (EMD Millipore Corp., catalog 05-753); rabbit anti-WT1 (Santa Cruz Biotechnology, catalog sc-192); mouse anti-HDAC1 (catalog 5356), mouse anti-HDAC2 (catalog 5113), rabbit anti–serum response factor (anti-SRF) (catalog 5147), rabbit anti–CRE-binding protein (anti-CREB) (catalog 9197), rabbit anti–phosphorylated CREB (Ser133) (catalog 9198), rabbit anti-EGR1 (catalog 4154), and rabbit anti-GAPDH (catalog 5174) (Cell Signaling Technology); mouse anti–talin-1 (Bio-Rad, catalog MCA4770); guinea pig anti-nephrin (Progen, catalog GP-N2); rabbit anti-EGR1 (Protein Tech, catalog 55117-1-AP); Alexa Fluor 594 phalloidin (catalog A12381), Alexa Fluor 488 goat anti-mouse IgG antibody (catalog A-11001), Alexa Fluor 594 goat anti–guinea pig IgG antibody (catalog A-11076), and Alexa Fluor 594 goat anti-rabbit IgG antibody (catalog A-11037) (Invitrogen) were purchased commercially. eGFP-EGR1 plasmid was purchased from Addgene.

Generation of mice. *Pod-rtTA TetO-Cre* mice on a C57BL/6 background were a gift from Alda Tufro (Yale University) (70). The mice were mated with our *Tln1*$^{fl/fl}$ mice on a C57BL/6 background (20) to generate doxycycline-inducible podocyte-specific *Tln1*-knockout mice (*Tln1*$^{fl/fl}$ *Pod-rtTA TetO-Cre* mice). Valproic acid (VPA) (Epigentek) (150 μg) or vorinostat (suberanilohydroxamic acid [SAHA]) (Sigma-Aldrich) (20 mg/kg body weight) was administered i.p. for 4 weeks after completion of doxycycline induction. *Hdac1*$^{fl/fl}$, *Hdac2*$^{fl/fl}$ mice were obtained as a gift from Eric Olson (University of Texas Southwestern Medical Center, Dallas, Texas, USA) (71), and the mice were mated with *Pod-rtTA TetO-Cre* mice or *Tln1*$^{fl/fl}$ *Pod-rtTA TetO-Cre* mice to generate doxycycline-inducible podocyte-specific *Hdac1*- and *Hdac2*-KO mice (*Hdac1*$^{fl/fl}$ *Hdac2*$^{fl/fl}$ *Pod-rtTA TetO-Cre* mice) or *Hdac1*-, *Hdac2*-, and *Tln1*-KO mice (*Hdac1*$^{fl/fl}$ *Hdac2*$^{fl/fl}$ *Tln1*$^{fl/fl}$ *Pod-rtTA TetO-Cre* mice). *Egr1*$^{+/-}$ mice on a C57BL/6 × 129 background were purchased from The Jackson Laboratory, and the mice were mated with *Pod-Cre Rosa-DTR*^{flox} mice on a C57BL/6 background, a gift from Lloyd Cantley (Yale University) (72), or *Tln1*$^{fl/fl}$ *Pod-rtTA TetO-Cre* mice to generate *Egr1*$^{-/-}$ *Pod-Cre Rosa-DTR*^{flox} mice and *Egr1*$^{-/-}$ *Tln1*$^{fl/fl}$ *Pod-rtTA*

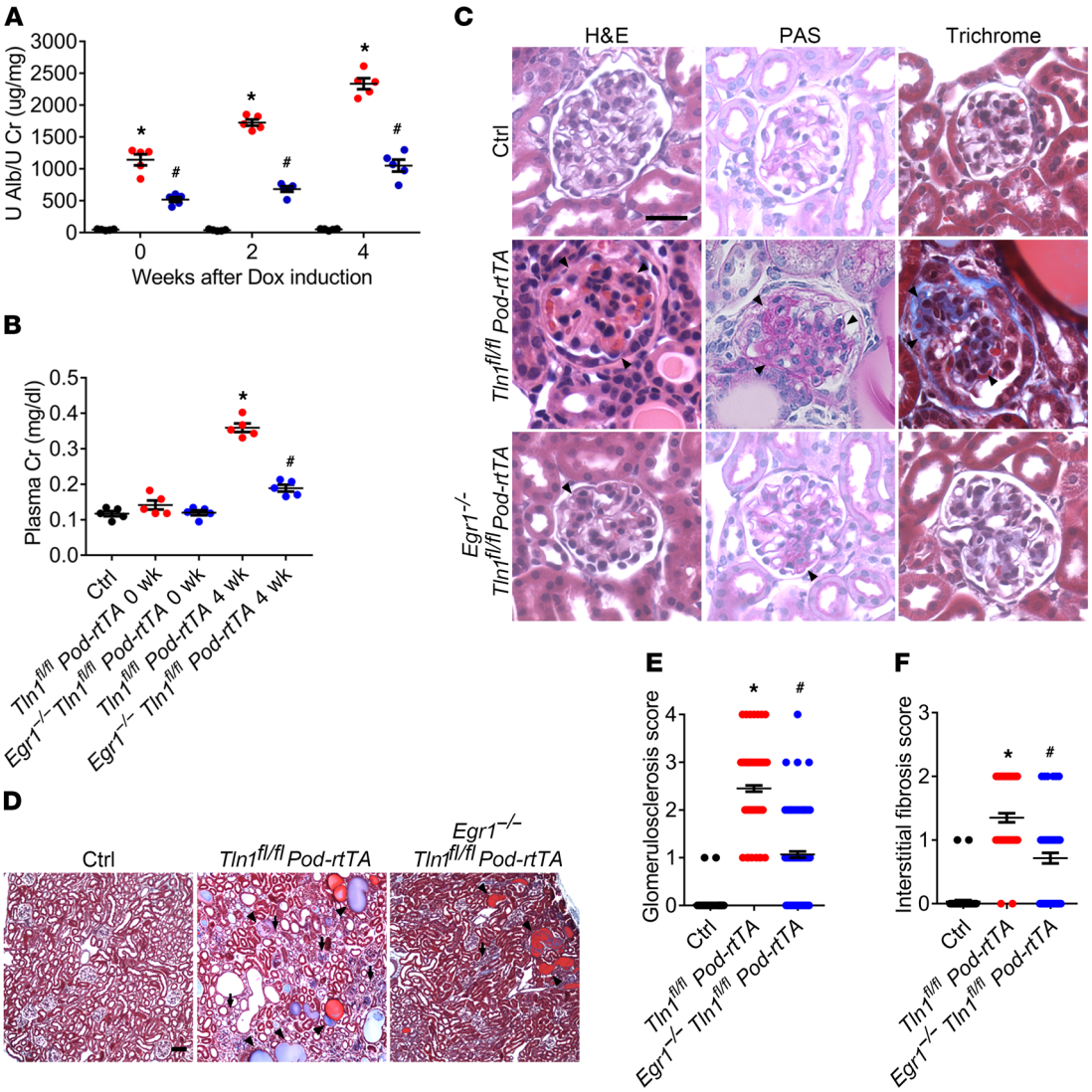

Figure 8. Loss of EGR1 in *Tln1*$^{fl/fl}$ *Pod-rtTA TetO-Cre* mice improves glomerulosclerosis and interstitial fibrosis. (**A**) Quantification of urine albumin/creatinine ratio in control (black), *Tln1*$^{fl/fl}$ *Pod-rtTA TetO-Cre* (red), and *Egr1*$^{-/-}$ *Tln1*$^{fl/fl}$ *Pod-rtTA TetO-Cre* (blue) mice at 0, 2, and 4 weeks after completion of Dox induction. **P* < 0.05 vs. control mice, #*P* < 0.05 vs. *Tln1*$^{fl/fl}$ *Pod-rtTA TetO-Cre* mice; *n* = 5. (**B**) Plasma creatinine in control, *Tln1*$^{fl/fl}$ *Pod-rtTA TetO-Cre*, and *Egr1*$^{-/-}$ *Tln1*$^{fl/fl}$ *Pod-rtTA TetO-Cre* mice 0 and 4 weeks after completion of Dox induction. **P* < 0.05 vs. control mice, #*P* < 0.05 vs. *Tln1*$^{fl/fl}$ *Pod-rtTA TetO-Cre* mice; *n* = 5. (**C**) Representative light microscope images (H&E, PAS, and trichrome) of glomeruli from control, *Tln1*$^{fl/fl}$ *Pod-rtTA TetO-Cre*, and *Egr1*$^{-/-}$ *Tln1*$^{fl/fl}$ *Pod-rtTA TetO-Cre* mice 4 weeks after completion of Dox induction. Arrowheads show mesangial matrix deposition and mesangial cell proliferation. Scale bar: 25 μm. (**D**) Representative trichrome staining in control, *Tln1*$^{fl/fl}$ *Pod-rtTA TetO-Cre*, and *Egr1*$^{-/-}$ *Tln1*$^{fl/fl}$ *Pod-rtTA TetO-Cre* mouse kidneys 4 weeks after completion of Dox induction. Arrowheads show dilated tubules and proteinaceous casts; arrows display interstitial fibrosis. Scale bar: 50 μm. (**E**) Quantification of glomerulosclerosis in **C**. **P* < 0.05 vs. control mice, #*P* < 0.05 vs. *Tln1*$^{fl/fl}$ *Pod-rtTA TetO-Cre* mice. (**F**) Quantification of interstitial fibrosis in **D**. **P* < 0.05 vs. control mice, #*P* < 0.05 vs. *Tln1*$^{fl/fl}$ *Pod-rtTA TetO-Cre* mice. (**A**, **B**, **E**, and **F**) Statistically analyzed by 1-way ANOVA with Dunnett's correction.

TetO-Cre mice, respectively. All generated mice were backcrossed more than 10 times before experiments. For podocyte injury models in vivo, nephrotoxic serum (NTS) (150 μl) was injected i.v. 5 days after adjuvant injection i.p. in control C57BL/6 mice at 8 weeks of age with or without i.p. VPA or SAHA administration 3 days after NTS injection. For another podocyte injury model, adriamycin (Sigma-Aldrich) (15 mg/kg body weight) was injected i.v. in 8-week-old BALB/c mice (The Jackson Laboratory), and VPA or SAHA was administered 7 days after adriamycin injection for 3 weeks.

Biochemical measurements, urine albumin, urine creatinine, and plasma creatinine. Mouse urine samples were collected at various ages. Urine albumin was quantified in duplicates using an Albumin ELISA Quantitation kit according to the manufacturer's protocol (Bethyl Laboratories Inc.). Plasma and urine creatinine were measured in duplicate for each sample at the time points above using a colorimetric quantification kit (Bioassay Systems) at an absorbance of 490 nm (Microplate Reader; Bio-Rad).

Cell culture. Isolation of podocytes from day 1–3 control and *Egr1*$^{-/-}$ *Pod-Cre Rosa-DTR*^{flox} pups was performed as described previously (72). Medium including diphtheria toxin (Sigma-Aldrich) was changed every other day 2 days after seeding of glomerular cells as previously described (72). Podocytes in culture were pretreated with VPA (0.5

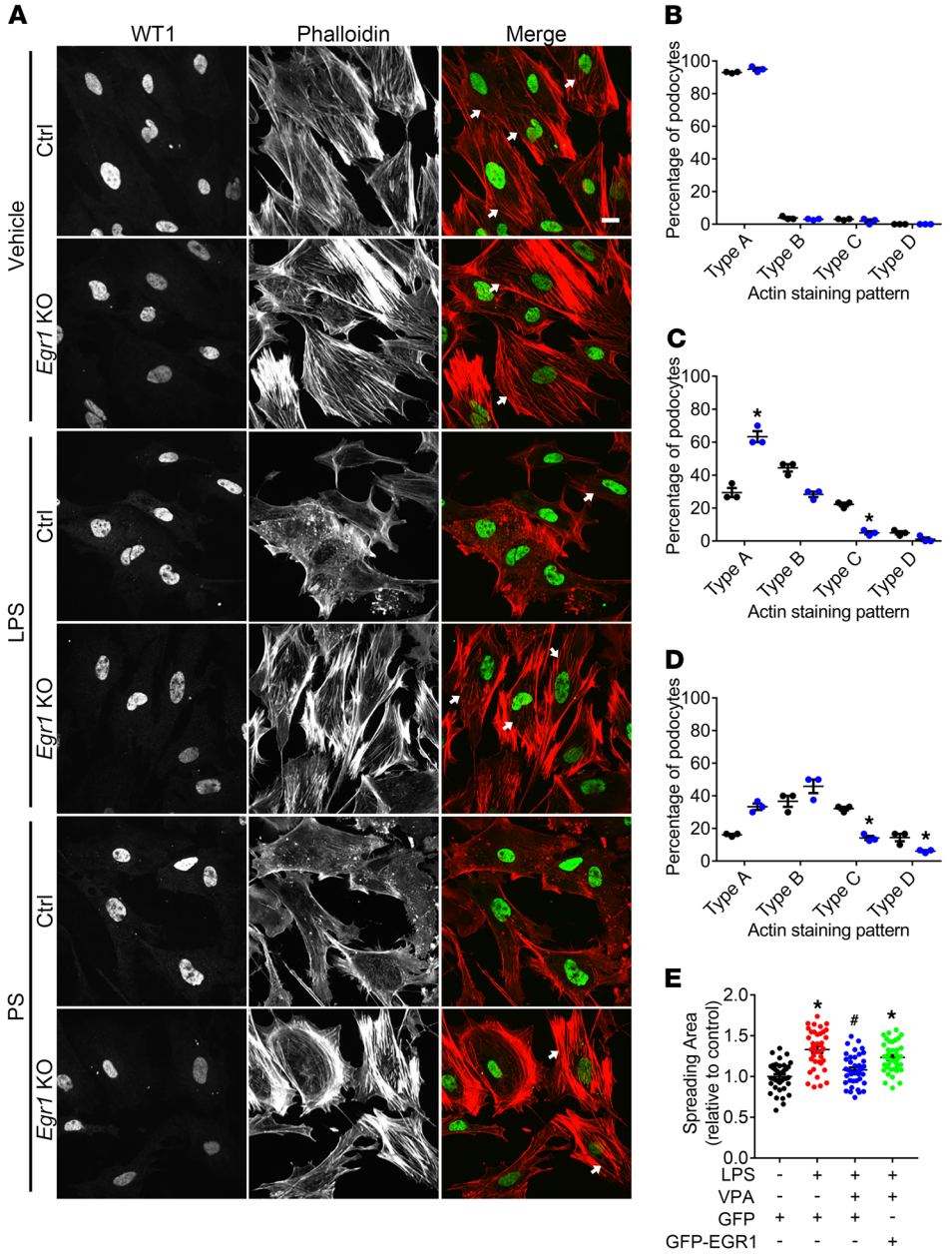

Figure 9. Loss of EGR1 stabilizes and maintains actin stress fibers following LPS or PS treatment. (**A**) Representative immunostaining for phalloidin (red) and WT1 (green) in control *Pod-Cre Rosa-DTR*^{flox} or *Egr1*$^{-/-}$ *Pod-Cre Rosa-DTR*^{flox} mouse primary podocytes treated with LPS or PS. Scale bar: 10 μm. (**B**–**D**) Quantification of phalloidin staining in control (black) or *Egr1*$^{-/-}$ *Pod-Cre Rosa-DTR*^{flox} (blue) mouse primary podocytes with vehicle (**B**), LPS (**C**), and PS (**D**). **P* < 0.05 vs. control mouse primary podocytes; *n* = 3. (**E**) Cell surface area in primary podocytes overexpressing GFP or GFP-EGR1 following LPS with or without VPA treatment. **P* < 0.05 vs. control primary podocytes, #*P* < 0.05 vs. LPS-treated primary podocytes; *n* = 3. Panels **C** and **D** statistically analyzed by 2-tailed Student's *t* test. Panel **E** statistically analyzed by 1-way ANOVA with Dunnett's correction.

mM) or SAHA (1 μM) and treated with 70 μg/ml lipopolysaccharide (LPS) (Sigma-Aldrich) or 20 μg/ml protamine sulfate (PS) (Sigma-Aldrich) at the designated time points.

Microarray of glomerular DNA and bioinformatics analysis. Glomeruli were isolated in control and *Tln1*$^{fl/fl}$ *Pod-rtTA TetO-Cre* mice 2 weeks after completion of doxycycline induction with or without VPA treatment. The glomerular RNA was isolated by RNeasy kit (Qiagen) and was sent to the Yale Center for Genome Analysis for microarray on the Affymetrix Mouse Genome 430 2.0 platform.

We used the R Bioconductor package to analyze the raw microarray gene expression data sets. Background for each data set was corrected using the RMA algorithm in the limma package. Probes were mapped to gene symbols using the annotation file downloaded from the Affymetrix website; probes with no annotation were discarded. The expression values in biological replicates were averaged. *Z* score for each gene was calculated as previously described (73). *Z* ratio of each gene was calculated by comparison of its expressions in different samples. The genes with absolute *Z* ratio value greater than 1.96 were identified as differentially expressed genes. These genes were shown in a 2-way hierarchical heatmap. Red and blue indicate up- and downregulated genes, respectively.

Upstream protein networks and pharmaceutical agents associated with the differentially expressed genes from control and *Tln1*$^{fl/fl}$ *Pod-rtTA TetO-Cre* mouse glomerulus microarray data sets were identified using Expression2Kinases (X2K) software (74). Briefly, X2K identified potential transcription factors regulating the differentially expressed genes using the ChIP-X Enrichment Analysis database. The transcription factors are then connected using known protein interactions, constructing a transcriptional regulatory subnetwork. Finally, pharmaceutical agents are identified that may reverse changes of differentially expressed genes in this subnetwork.

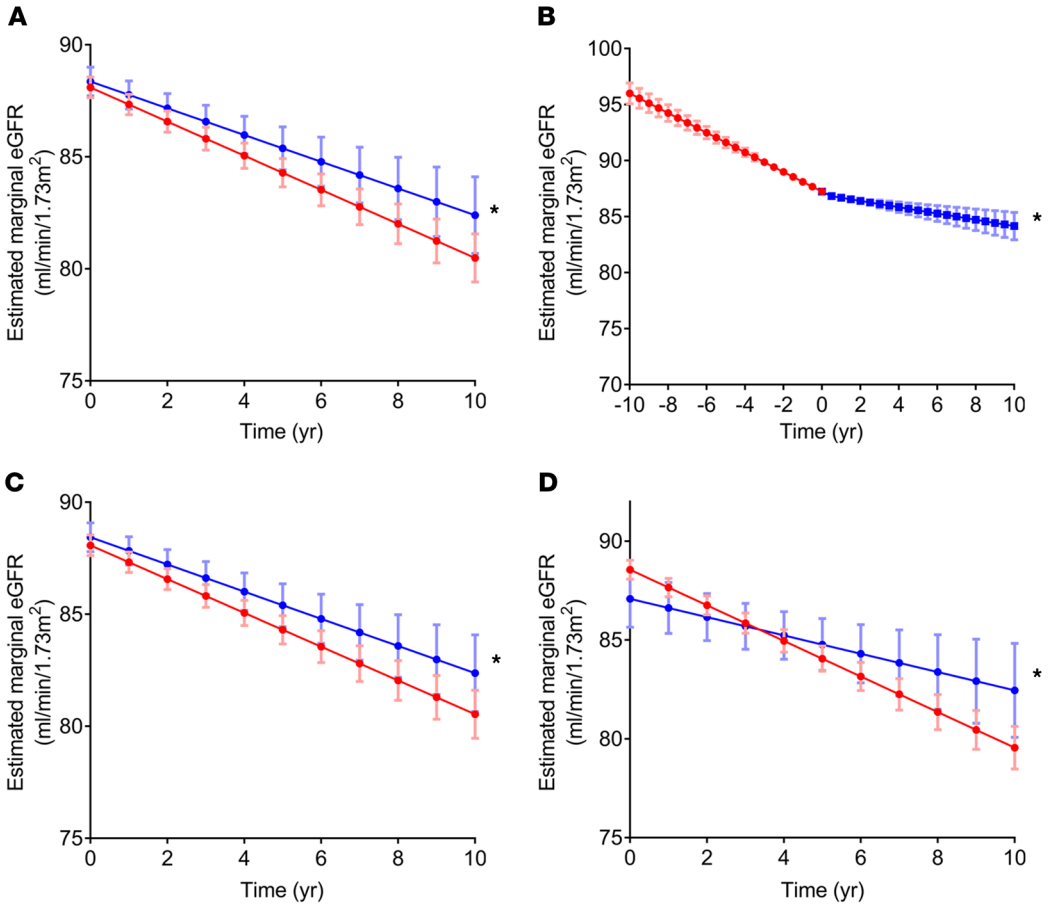

Figure 10. VPA usage is associated with slower declines in eGFR in a Veterans Affairs population cohort. (**A**) The slope of eGFR decline among patients treated with VPA compared with controls not treated with VPA. *P = 0.02. (**B**) The slope of eGFR decline in patients before and after initiation of VPA. *P <0.001. (**C** and **D**) The slope of eGFR decline among patients with no or mild proteinuria (1+ or below on urine dipstick) (**C**) and with heavy proteinuria (>2+ on urine dipstick) (**D**) with or without VPA. *P-for-interaction = 0.02. All graphs reflect eGFRs adjusted for age, sex, race, baseline eGFR, HCV, HIV, diabetes, hypertension, congestive heart failure, liver disease, bipolar disorder, depression, post-traumatic stress disorder, prior stroke, epilepsy, and headache. The visualized slopes reflect eGFR at the mode of categorical covariates and the mean of continuous covariates.

Quantitative PCR analysis. Total RNA was extracted from the primary podocytes or isolated glomeruli using Trizol (Thermo Fisher Scientific). The RNA concentration was measured by spectrophotometry (Nanodrop Technologies). The RNA (1 μg) was used for reverse transcription by a high-capacity cDNA Synthesis Kit according to the manufacturer's instructions (Applied Biosystems). The quantitative PCR amplifications were performed using Power SYBR Green PCR Master Mix (Applied Biosystems) with a 7300 AB real-time PCR machine (Applied Biosystems).

Immunoblotting. Primary podocytes or isolated glomeruli were lysed in lysis buffer containing 50 mM Tris-HCl (pH 7.6), 500 mM NaCl, 0.1% SDS, 0.5 % deoxycholate, 1 % Triton X-100, 0.5 mM $MgCl_2$, 1 mM Na_3VO_4, 50 mM NaF, 1 mM PMSF, protease inhibitor cocktail (Roche Diagnostics), and phosphatase inhibitor cocktail (MilliporeSigma). Protein concentrations were quantified using the Bio-Rad protein assay. Equal amounts of lysates were separated by SDS-PAGE and transferred on PVDF membranes (EMD Millipore Corp.). The membrane was blocked with 5% nonfat milk (American Bio) or 3% BSA (Sigma-Aldrich) in Tris-buffered saline and Tween-20 (TBS-T) and incubated with the appropriate primary antibody at 4°C overnight. After 3 washes with TBS-T, the appropriate peroxidase-labeled anti-IgG secondary antibody (Millipore) was added and signals detected using enhanced chemiluminescence reagents (Bio-Rad) and exposed with Odyssey (LI-COR Biosciences). For quantification, densitometry was performed using ImageJ software (NIH).

ChIP assay. Primary podocytes were cross-linked by 1 % formaldehyde, and ChIP assay was performed using CREB or SRF antibody with a SimpleChIP Kit according to the manufacturer's protocol (Cell Signaling Technology). Coprecipitated DNA and input DNA were quantified by reverse transcriptase PCR calculating as the ratio of PCR signal from coprecipitated DNA to that from input DNA. As the mouse *Egr1* gene promoter contains 5 serum response elements (SREs) and 2 cAMP response elements (CREs) and the CREs and the first 2 SREs are close, we generated primers in the mouse *Egr1* promoter as follows: primer set 1 (for CREs and the first 2 SREs) forward 5′-TTTCCAGGAGCCTGAGCGC-3′, reverse 5′-CCCGAATCGGCCTCTATTTCA-3′; primer set 2 (for the other SREs) forward 5′-CCGACCCGGAAACGCCATAT-3′, reverse 5′-TCCTCCCAGAGCCGGAAA-3′.

HDAC1 and HDAC2 activity assays. Mouse glomeruli were isolated, followed by podocyte enrichment by sieving through a 40-μm cell strainer. Nuclear protein was extracted using NE-PER Nuclear and Cytoplasmic Extraction Reagents (Thermo Fisher Scientific). Total HDAC activity was measured using an Epigenase HDAC Activity/Inhibition Direct Assay Kit according to the manufacturer's protocol (Epigentek). Each HDAC1 and HDAC2 activity was measured using an HDAC1 or HDAC2 Immunoprecipitation & Activity Assay Kit, respectively, according to the manufacturer's protocol (BioVision).

Kidney histology and quantification. Mice were anesthetized by i.p. injection of ketamine and xylazine followed by perfusion fixation with 4% paraformaldehyde with or without 2% glutaraldehyde through the left ventricle. Sections were stained for H&E, periodic acid–Schiff, and Masson's trichrome staining by the Yale Pathology Core Tissue Services. To evaluate glomerulosclerosis and interstitial fibrosis, kidney sections with Masson's trichrome staining were assessed as previously

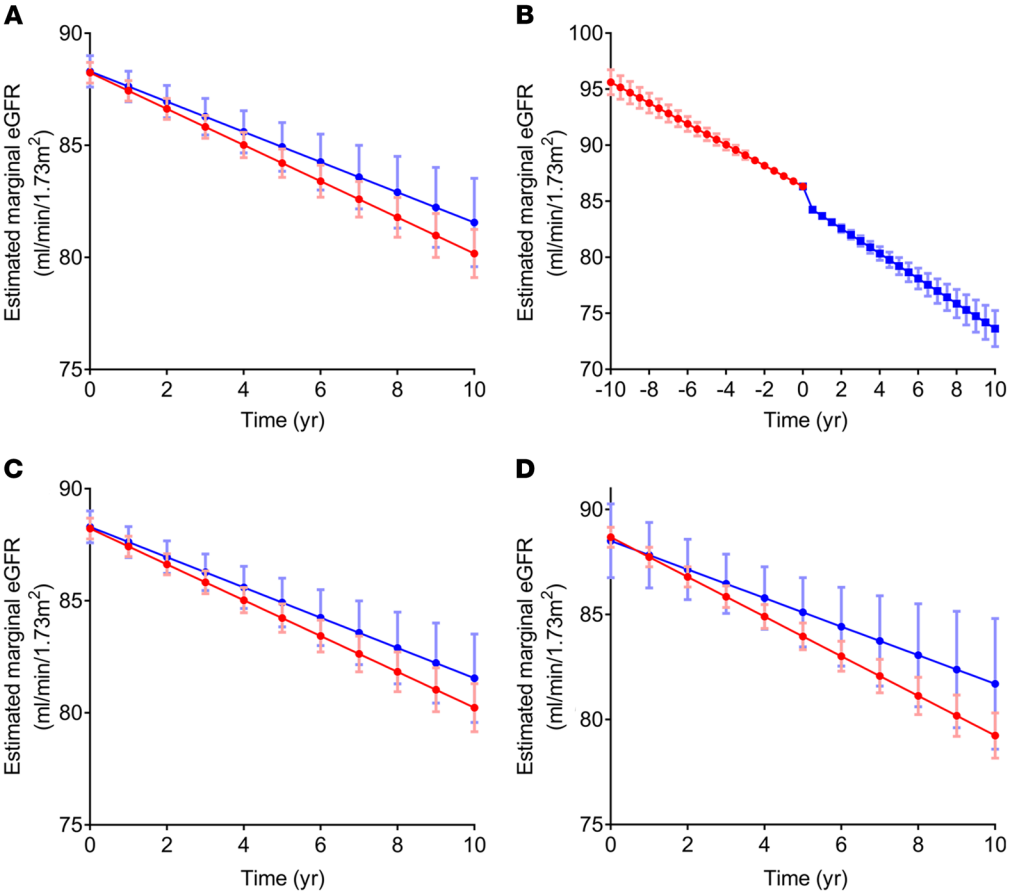

Figure 11. Usage of comparator drugs (lamotrigine, carbamazepine, and levetiracetam) is not associated with declines in eGFR in a Veterans Affairs population cohort. (**A**) The slope of eGFR decline among patients treated with comparator drugs compared with controls not treated with comparator drugs. (**B**) The slope of eGFR decline in patients before and after initiation of comparator drugs. (**C** and **D**) The slope of eGFR decline among patients with no or mild proteinuria (1+ or below on urine dipstick) (**C**) and with heavy proteinuria (>2+ on urine dipstick) (**D**) with or without comparator drugs. All graphs reflect eGFRs adjusted for age, sex, race, baseline eGFR, HCV, HIV, diabetes, hypertension, congestive heart failure, liver disease, bipolar disorder, depression, post-traumatic stress disorder, prior stroke, epilepsy, and headache. The visualized slopes reflect eGFR at the mode of categorical covariates and the mean of continuous covariates.

described (75). The number of foot processes was divided by the total length of glomerular basement membrane regions in each electron microscopic image (76). In all histological analysis, 3 different mice were used in independent experiments.

Immunofluorescence staining. Primary podocytes on collagen I–coated coverslips were washed by PBS and fixed with 4% paraformaldehyde for 15 minutes. The cells were permeabilized with 0.1% Triton X in PBS for 5 minutes, followed by blocking with 3% BSA in PBS for 1 hour. For human kidney biopsy samples, paraffin-embedded kidney sections were deparaffinized by xylene following hydration by ethanol. For both human and mouse kidney sections, antigen retrieval was induced by microwave following washing with PBS, and kidney sections were blocked with 3% BSA in PBS. Immunostaining was performed with primary antibodies overnight at 4°C, followed by Alexa Fluor 488– and/or Alexa Fluor 594–conjugated secondary antibodies, and then cells were washed with PBS and mounted with Slowfade (Invitrogen). TUNEL staining was performed using an In Situ Cell Death Detection Kit according to the manufacturer's protocol (Roche). In each immunofluorescence staining, 3 different mice or podocytes were used. Images were taken by an Andor CSU-WDi spinning disc confocal microscope equipped with a Nikon Ti-E CFI Plan Apochromat Lambda ×60 oil immersion objective for immunofluorescence analysis, and images were processed using NIH ImageJ software (version 1.51H) or Adobe Photoshop CS 2014. For quantification of podocyte number, WT1-positive nuclei were counted in each glomeruli (77). For quantification of changes in actin cytoarchitecture of primary podocytes, podocytes stained with phalloidin were grouped into 4 major classes, which were used for scoring as described previously (type A: more than 90% of cell area filled with thick cables; type B: at least 2 thick cables running under nucleus and rest of cell area filled with fine cables; type C: no thick cables, but some cables present; type D: no cables visible in the central area of the cell) (20, 78). One hundred primary podocytes from each mouse were analyzed in 3 independent experiments.

Cell spreading. Following overexpression of GFP or GFP-EGR1 in control podocytes, cells were detached by trypsin digestion. The cell suspension was placed on collagen I–coated coverslips, and the cells were treated with LPS (3 hours) with or without VPA. The primary podocytes were fixed with 4% paraformaldehyde and stained with GFP and phalloidin. The cell surface area was measured in GFP-positive primary podocytes using NIH ImageJ software.

Human study. Participants in the Veterans Aging Cohort Study (VACS) were considered for enrollment. The VACS is a longitudinal cohort study of 141,686 HIV-positive veterans and an age/race/site-matched sample of uninfected controls (79). For the present analysis, we included VACS participants with at least 2 outpatient creatinine values measured at least 1 year apart to allow for calculation of a slope of eGFR. GFR was estimated using the CKD-Epi formula (80). VPA exposure during a creatinine interval was defined as the presence of a VPA prescription for more than 50% of the days between 2 consecutive creatinine measurements.

A patient time period (bounded by sequential creatinine measurements) was classified as "exposed to VPA" if the patient had an active prescription for VPA for at least 50% of that period.

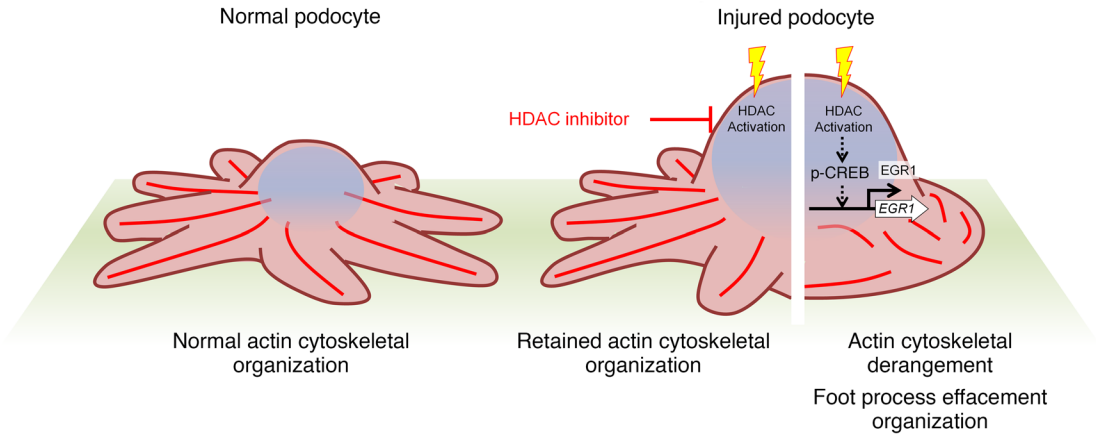

Figure 12. Cartoon schematic shows that HDAC activation results in actin cytoskeleton derangement and progression of podocyte injury through p-CREB–induced EGR1 upregulation.

We compared covariates across groups using Student's *t* test or χ^2 tests as appropriate. The primary statistical analysis used a mixed-effects model with random slopes and random intercepts. Time periods were bounded by creatinine measurements. To estimate the slope of eGFR, time interaction terms were included in the model. The fixed component of the model was used to assess between individual effects of VPA, while the random component was used to assess within individual effects. All models were adjusted for baseline eGFR, age, sex, race, presence of HIV, presence of hepatitis C, diabetes, hypertension, congestive heart failure, liver disease, bipolar disorder, depression, post-traumatic stress disorder, prior stroke, epilepsy, and headache. We ascertained comorbidities using ICD-9 codes (81).

The predefined comparator agents were lamotrigine, carbamazepine, and levetiracetam. Owing to sparse numbers for these agents, exposure to these medications was combined into a single "comparator medication exposure" variable. Lithium use was coded as an "ever exposed" versus "never exposed" variable. Patients with any lithium exposure were excluded from a sensitivity analysis to ensure that the observed benefit of VPA administration was not due to the withdrawal of lithium.

Data availability. The microarray data used in this study were deposited in the NCBI's Gene Expression Omnibus database under accession code GSE112116.

Statistics. Data are displayed as the mean ± SEM. The number of replicates for each experiment is shown in Methods or the figure legends. Statistical differences between 2 groups were evaluated by a 2-tailed *t* test. Multiple-group comparisons were evaluated using 1-way ANOVA followed by Dunnett's multiple-comparisons tests. Statistical analysis was performed by GraphPad Prism 7 software. A *P* value less than 0.05 was considered statistically significant. For human data, statistical significance was determined with a 2-sided *P* value less than 0.05 for primary effects and less than 0.10 for interaction tests. Analyses were performed in Stata v15.0 (StataCorp) and SAS version 9.4 (SAS Institute).

Study approval. The Yale University IACUC approved all animal experiments, and the Veterans Affairs IRB (West Haven, CT) approved the analysis of VACS data. All work was carried on in accordance with the principles and procedures outlined in the NIH guidelines for the care and use of experimental animals.

Author contributions

KI and SI designed research studies. KI, GG, MC, CEP, and XT conducted experiments. KI, GG, MC, XT, CC, JT, and AJ acquired data. YZ and ZZ analyzed microarray data. KI, CEP, YW, EC, MG, NC, ZW, CRP, FPW, and SI analyzed the data. FPW and SI wrote the manuscript.

Acknowledgments

The work was supported by NIH grants DK083294 and DK093269, Department of Defense grant W81XWH-17-1-0662 to SI, and the George O'Brien Kidney Center at Yale (P30 DK079310).

Address correspondence to: Shuta Ishibe, Section of Nephrology, Yale University School of Medicine, PO Box 208029, 333 Cedar Street, New Haven, Connecticut 06520-8029, USA. Phone: 203.737.4170; Email: shuta.ishibe@yale.edu.

1. Moeller MJ, Tenten V. Renal albumin filtration: alternative models to the standard physical barriers. *Nat Rev Nephrol*. 2013;9(5):266–277.
2. Scott RP, Quaggin SE. Review series: The cell biology of renal filtration. *J Cell Biol*. 2015;209(2):199–210.
3. Eckardt KU, et al. Evolving importance of kidney disease: from subspecialty to global health burden. *Lancet*. 2013;382(9887):158–169.
4. Kramer A, et al. The European Renal Association – European Dialysis and Transplant Association (ERA-EDTA) Registry Annual Report 2015: a summary. *Clin Kidney J*. 2018;11(1):108–122.
5. Maschio G, et al. Effect of the angiotensin-converting-enzyme inhibitor benazepril on the progression of chronic renal insufficiency. The Angiotensin-Converting-Enzyme Inhibition in Progressive Renal Insufficiency Study Group. *N Engl J Med*. 1996;334(15):939–945.
6. Lamb J, et al. The Connectivity Map: using gene-expression signatures to connect small molecules, genes, and disease. *Science*. 2006;313(5795):1929–1935.
7. Xiu Y, et al. Stabilization of NF-κB-inducing kinase suppresses MLL-AF9-induced acute myeloid leukemia. *Cell Rep*. 2018;22(2):350–358.
8. Zhong Y, et al. Renoprotective effect of combined inhibition of angiotensin-converting enzyme and histone deacetylase. *J Am Soc Nephrol*. 2013;24(5):801–811.
9. Eberharter A, Becker PB. Histone acetylation: a switch between repressive and permissive chromatin. Second in review series on chromatin

dynamics. *EMBO Rep*. 2002;3(3):224–229.
10. Narlikar GJ, Fan HY, Kingston RE. Cooperation between complexes that regulate chromatin structure and transcription. *Cell*. 2002;108(4):475–487.
11. Wang Z, et al. Genome-wide mapping of HATs and HDACs reveals distinct functions in active and inactive genes. *Cell*. 2009;138(5):1019–1031.
12. Minucci S, Pelicci PG. Histone deacetylase inhibitors and the promise of epigenetic (and more) treatments for cancer. *Nat Rev Cancer*. 2006;6(1):38–51.
13. Glozak MA, Sengupta N, Zhang X, Seto E. Acetylation and deacetylation of non-histone proteins. *Gene*. 2005;363:15–23.
14. Thompson PR, et al. Regulation of the p300 HAT domain via a novel activation loop. *Nat Struct Mol Biol*. 2004;11(4):308–315.
15. Houtkooper RH, Pirinen E, Auwerx J. Sirtuins as regulators of metabolism and healthspan. *Nat Rev Mol Cell Biol*. 2012;13(4):225–238.
16. Haberland M, Montgomery RL, Olson EN. The many roles of histone deacetylases in development and physiology: implications for disease and therapy. *Nat Rev Genet*. 2009;10(1):32–42.
17. Kong Y, et al. Suppression of class I and II histone deacetylases blunts pressure-overload cardiac hypertrophy. *Circulation*. 2006;113(22):2579–2588.
18. Tang Y, et al. Inhibiting histone deacetylase 2 (HDAC2) promotes functional recovery from stroke. *J Am Heart Assoc*. 2017;6(10):e007236.
19. Choong CJ, et al. A novel histone deacetylase 1 and 2 isoform-specific inhibitor alleviates experimental Parkinson's disease. *Neurobiol Aging*. 2016;37:103–116.
20. Tian X, et al. Podocyte-associated talin1 is critical for glomerular filtration barrier maintenance. *J Clin Invest*. 2014;124(3):1098–1113.
21. [No authors listed]. Sodium valproate in epilepsy. *Lancet*. 1977;2(8043):860.
22. Gram L, et al. Valproate sodium: a controlled clinical trial including monitoring of drug levels. *Epilepsia*. 1977;18(2):141–148.
23. Henry TR. The history of valproate in clinical neuroscience. *Psychopharmacol Bull*. 2003;37(suppl 2):5–16.
24. Mattson RH, Cramer JA, Williamson PD, Novelly RA. Valproic acid in epilepsy: clinical and pharmacological effects. *Ann Neurol*. 1978;3(1):20–25.
25. Jensen R, Brinck T, Olesen J. Sodium valproate has a prophylactic effect in migraine without aura: a triple-blind, placebo-controlled crossover study. *Neurology*. 1994;44(4):647–651.
26. Baker RW, et al. Efficacy of olanzapine combined with valproate or lithium in the treatment of dysphoric mania. *Br J Psychiatry*. 2004;185:472–478.
27. Duenas-Gonzalez A, Candelaria M, Perez-Plascencia C, Perez-Cardenas E, de la Cruz-Hernandez E, Herrera LA. Valproic acid as epigenetic cancer drug: preclinical, clinical and transcriptional effects on solid tumors. *Cancer Treat Rev*. 2008;34(3):206–222.
28. Mann BS, Johnson JR, Cohen MH, Justice R, Pazdur R. FDA approval summary: vorinostat for treatment of advanced primary cutaneous T-cell lymphoma. *Oncologist*. 2007;12(10):1247–1252.
29. Soda K, et al. Role of dynamin, synaptojanin, and endophilin in podocyte foot processes. *J Clin Invest*. 2012;122(12):4401–4411.
30. Tarcic G, et al. EGR1 and the ERK-ERF axis drive mammary cell migration in response to EGF. *FASEB J*. 2012;26(4):1582–1592.
31. Cermák V, Kosla J, Plachý J, Trejbalová K, Hejnar J, Dvorák M. The transcription factor EGR1 regulates metastatic potential of v-src transformed sarcoma cells. *Cell Mol Life Sci*. 2010;67(20):3557–3568.
32. Xie B, et al. Egr-1 transactivates Bim gene expression to promote neuronal apoptosis. *J Neurosci*. 2011;31(13):5032–5044.
33. Sakamoto KM, Bardeleben C, Yates KE, Raines MA, Golde DW, Gasson JC. 5′ upstream sequence and genomic structure of the human primary response gene, EGR-1/TIS8. *Oncogene*. 1991;6(5):867–871.
34. Tur G, Georgieva EI, Gagete A, López-Rodas G, Rodríguez JL, Franco L. Factor binding and chromatin modification in the promoter of murine Egr1 gene upon induction. *Cell Mol Life Sci*. 2010;67(23):4065–4077.
35. Duclot F, Kabbaj M. The role of early growth response 1 (EGR1) in brain plasticity and neuropsychiatric disorders. *Front Behav Neurosci*. 2017;11:35.
36. ENCODE Project Consortium. An integrated encyclopedia of DNA elements in the human genome. *Nature*. 2012;489(7414):57–74.
37. Koldamova R, et al. Genome-wide approaches reveal EGR1-controlled regulatory networks associated with neurodegeneration. *Neurobiol Dis*. 2014;63:107–114.
38. He F, et al. Sublytic C5b-9 triggers glomerular mesangial cell apoptosis in rat Thy-1 nephritis via Gadd45 activation mediated by Egr-1 and p300-dependent ATF3 acetylation. *J Mol Cell Biol*. 2016;8(6):477–491.
39. Grams ME, et al. Race, APOL1 risk, and eGFR decline in the general population. *J Am Soc Nephrol*. 2016;27(9):2842–2850.
40. Baba M, et al. Longitudinal study of the decline in renal function in healthy subjects. *PLoS One*. 2015;10(6):e0129036.
41. Levin NW, et al. Blood pressure in chronic kidney disease stage 5D-report from a kidney disease: improving global 0utcomes controversies conference. *Kidney Int*. 2010;77(4):273–284.
42. Saran R, et al. US Renal Data System 2016 Annual Data Report: Epidemiology of Kidney Disease in the United States. *Am J Kidney Dis*. 2017;69(3 suppl 1):A7–A8.
43. Rogers J, Taylor MJ. Pharmacological agents to reduce readmissions in bipolar disorder. *J Psychopharmacol (Oxford)*. 2017;31(3):387–388.
44. Zhang L, et al. Sodium butyrate protects against high fat diet-induced cardiac dysfunction and metabolic disorders in type II diabetic mice. *J Cell Biochem*. 2017;118(8):2395–2408.
45. Cianciolo Cosentino C, et al. Histone deacetylase inhibitor enhances recovery after AKI. *J Am Soc Nephrol*. 2013;24(6):943–953.
46. Liu N, et al. Blocking the class I histone deacetylase ameliorates renal fibrosis and inhibits renal fibroblast activation via modulating TGF-beta and EGFR signaling. *PLoS One*. 2013;8(1):e54001.
47. Van Beneden K, et al. Valproic acid attenuates proteinuria and kidney injury. *J Am Soc Nephrol*. 2011;22(10):1863–1875.
48. Montgomery RL, Hsieh J, Barbosa AC, Richardson JA, Olson EN. Histone deacetylases 1 and 2 control the progression of neural precursors to neurons during brain development. *Proc Natl Acad Sci U S A*. 2009;106(19):7876–7881.
49. Yamaguchi T, et al. Histone deacetylases 1 and 2 act in concert to promote the G1-to-S progression. *Genes Dev*. 2010;24(5):455–469.
50. Wang X, et al. Histone deacetylase 4 selectively contributes to podocyte injury in diabetic nephropathy. *Kidney Int*. 2014;86(4):712–725.
51. Liu F, et al. Silencing of histone deacetylase 9 expression in podocytes attenuates kidney injury in diabetic nephropathy. *Sci Rep*. 2016;6:33676.
52. Mechtcheriakova D, et al. Specificity, diversity, and convergence in VEGF and TNF-alpha signaling events leading to tissue factor up-regulation via EGR-1 in endothelial cells. *FASEB J*. 2001;15(1):230–242.
53. Chang JS, et al. Oxygen deprivation triggers upregulation of early growth response-1 by the receptor for advanced glycation end products. *Circ Res*. 2008;102(8):905–913.
54. Ohtani K, et al. Inhibition of neointimal hyperplasia after balloon injury by cis-element 'decoy' of early growth response gene-1 in hypercholesterolemic rabbits. *Gene Ther*. 2004;11(2):126–132.
55. Hofer G, Grimmer C, Sukhatme VP, Sterzel RB, Rupprecht HD. Transcription factor Egr-1 regulates glomerular mesangial cell proliferation. *J Biol Chem*. 1996;271(45):28306–28310.
56. Carl M, Akagi Y, Weidner S, Isaka Y, Imai E, Rupprecht HD. Specific inhibition of Egr-1 prevents mesangial cell hypercellularity in experimental nephritis. *Kidney Int*. 2003;63(4):1302–1312.
57. Ho LC, et al. Egr-1 deficiency protects from renal inflammation and fibrosis. *J Mol Med*. 2016;94(8):933–942.
58. Nakamura H, et al. Introduction of DNA enzyme for Egr-1 into tubulointerstitial fibroblasts by electroporation reduced interstitial alpha-smooth muscle actin expression and fibrosis in unilateral ureteral obstruction (UUO) rats. *Gene Ther*. 2002;9(8):495–502.
59. Muthukkumar S, Nair P, Sells SF, Maddiwar NG, Jacob RJ, Rangnekar VM. Role of EGR-1 in thapsigargin-inducible apoptosis in the melanoma cell line A375-C6. *Mol Cell Biol*. 1995;15(11):6262–6272.
60. Kim SO, et al. Anti-invasive activity of histone deacetylase inhibitors via the induction of Egr-1 and the modulation of tight junction-related proteins in human hepatocarcinoma cells. *BMB Rep*. 2009;42(10):655–660.
61. Su L, Cheng H, Sampaio AV, Nielsen TO, Underhill TM. EGR1 reactivation by histone deacetylase inhibitors promotes synovial sarcoma cell death through the PTEN tumor suppressor. *Oncogene*. 2010;29(30):4352–4361.
62. Subburaju S, Coleman AJ, Ruzicka WB, Benes FM. Toward dissecting the etiology of schizophrenia: HDAC1 and DAXX regulate GAD67 expression in an in vitro hippocampal GABA neuron model. *Transl Psychiatry*. 2016;6:e723.
63. Delghandi MP, Johannessen M, Moens U. The

cAMP signalling pathway activates CREB through PKA, p38 and MSK1 in NIH 3T3 cells. *Cell Signal*. 2005;17(11):1343–1351.
64. Gonzalez AA, et al. PKC-α-dependent augmentation of cAMP and CREB phosphorylation mediates the angiotensin II stimulation of renin in the collecting duct. *Am J Physiol Renal Physiol*. 2015;309(10):F880–F888.
65. Ma H, et al. γCaMKII shuttles Ca^{2}[+]/CaM to the nucleus to trigger CREB phosphorylation and gene expression. *Cell*. 2014;159(2):281–294.
66. Davis S, Vanhoutte P, Pages C, Caboche J, Laroche S. The MAPK/ERK cascade targets both Elk-1 and cAMP response element-binding protein to control long-term potentiation-dependent gene expression in the dentate gyrus in vivo. *J Neurosci*. 2000;20(12):4563–4572.
67. Du K, Montminy M. CREB is a regulatory target for the protein kinase Akt/PKB. *J Biol Chem*. 1998;273(49):32377–32379.
68. Gu T, Zhang Z, Wang J, Guo J, Shen WH, Yin Y. CREB is a novel nuclear target of PTEN phosphatase. *Cancer Res*. 2011;71(8):2821–2825.
69. Pan L, et al. Histone deacetylase inhibitor trichostatin a potentiates doxorubicin-induced apoptosis by up-regulating PTEN expression. *Cancer*. 2007;109(8):1676–1688.
70. Veron D, et al. Induction of podocyte VEGF164 overexpression at different stages of development causes congenital nephrosis or steroid-resistant nephrotic syndrome. *Am J Pathol*. 2010;177(5):2225–2233.
71. Montgomery RL, et al. Histone deacetylases 1 and 2 redundantly regulate cardiac morphogenesis, growth, and contractility. *Genes Dev*. 2007;21(14):1790–1802.
72. Guo JK, et al. The Terminator mouse is a diphtheria toxin-receptor knock-in mouse strain for rapid and efficient enrichment of desired cell lineages. *Kidney Int*. 2013;84(5):1041–1046.
73. Cheadle C, Vawter MP, Freed WJ, Becker KG. Analysis of microarray data using Z score transformation. *J Mol Diagn*. 2003;5(2):73–81.
74. Chen EY, Xu H, Gordonov S, Lim MP, Perkins MH, Ma'ayan A. Expression2Kinases: mRNA profiling linked to multiple upstream regulatory layers. *Bioinformatics*. 2012;28(1):105–111.
75. Hassan H, et al. Essential role of X-box binding protein-1 during endoplasmic reticulum stress in podocytes. *J Am Soc Nephrol*. 2016;27(4):1055–1065.
76. Ma H, et al. Inhibition of podocyte FAK protects against proteinuria and foot process effacement. *J Am Soc Nephrol*. 2010;21(7):1145–1156.
77. Hassan H, et al. Essential role of X-box binding protein-1 during endoplasmic reticulum stress in podocytes. *J Am Soc Nephrol*. 2016;27(4):1055–1065.
78. Verderame M, Alcorta D, Egnor M, Smith K, Pollack R. Cytoskeletal F-actin patterns quantitated with fluorescein isothiocyanate-phalloidin in normal and transformed cells. *Proc Natl Acad Sci U S A*. 1980;77(11):6624–6628.
79. Justice AC, et al. Veterans Aging Cohort Study (VACS): overview and description. *Med Care*. 2006;44(8 suppl 2):S13–S24.
80. Levey AS, et al. A new equation to estimate glomerular filtration rate. *Ann Intern Med*. 2009;150(9):604–612.
81. Quan H, et al. Coding algorithms for defining comorbidities in ICD-9-CM and ICD-10 administrative data. *Med Care*. 2005;43(11):1130–1139.